อนุภาคระดับนาโนเมตรของพอลิแอนิลีนนำไฟฟ้ากักเก็บด้วยพอลิอะคริเลต ผ่านซีดอิมัลชันพอลิเมอไรเซชันแบบปราศจากอิมัลซิฟายเออร์

นางสาวพรรณระพี วรเกริกกุลชัย

วิทยานิพนธ์นี้เป็นส่วนหนึ่งของการศึกษาตามหลักสูตรปริญญาวิทยาศาสตรมหาบัณฑิต
สาขาวิชาปิโตรเคมีและวิทยาศาสตร์พอลิเมอร์
คณะวิทยาศาสตร์ จุฬาลงกรณ์มหาวิทยาลัย
ปีการศึกษา 2556

CONDUCTING POLYANILINE NANOPARTICLES ENCAPSULATED WITH POLYACRYLATE VIA EMULSIFIER FREE SEEDED EMULSION POLYMERIZATION

Miss Phanrapee Varakirkkulchai

A Thesis Submitted in Partial Fulfillment of the Requirements
for the Degree of Master of Science Program in Petrochemistry and Polymer Science
Faculty of Science
Chulalongkorn University
Academic Year 2013

Thesis Title	CONDUCTING POLYANILINE NANOPARTICLES ENCAPSULATED WITH POLYACRYLATE VIA EMULSIFIER FREE SEEDED EMULSION POLYMERIZATION
By	Miss Phanrapee Varakirkkulchai
Field of Study	Petrochemistry and Polymer Science
Thesis Advisor	Professor Pattarapan Prasassarakich, Ph.D.
Thesis Co-advisor	Suwadee Kongparakul, Ph.D.

Accepted by the Faculty of Science, Chulalongkorn University in Partial Fulfillment of the Requirements for the Master's Degree

..…….. Dean of the Faculty of Science
(Professor Supot Hannongbua, Dr.rer.nat.)

THESIS COMMITTEE

…….. Chairman
(Professor Tharapong Vitidsant, Ph.D.)

…….…… Thesis Advisor
(Professor Pattarapan Prasassarakich, Ph.D.)

…….…… Thesis Co-advisor
(Suwadee Kongparakul, Ph.D.)

…….. Examiner
(Associate Professor Nuanphun Chantarasiri, Ph.D.)

…….. External Examiner
(Associate Professor Ittipol Jangchud, Ph.D.)

พรรณระพี วรเกริกกุลชัย: อนุภาคระดับนาโนเมตรของพอลิแอนิลีนนำไฟฟ้ากักเก็บด้วยพอลิอะคริเลต ผ่านซีดอิมัลชันพอลิเมอไรเซชันแบบปราศจากอิมัลซิฟายเออร์. (CONDUCTING POLYANILINE NANOPARTICLES ENCAPSULATED WITH POLYACRYLATE VIA EMULSIFIER FREE SEEDED EMULSION POLYMERIZATION) อ.ที่ปรึกษาวิทยานิพนธ์หลัก: ศ.ดร.ภัทรพรรณ ประศาสน์สารกิจ, อ.ที่ปรึกษาวิทยานิพนธ์ร่วม: อ.ดร. สุวดี ก้องพารากุล, 86 หน้า.

การสังเคราะห์อนุภาคนาโนคอมพอสิตของพอลิแอนิลีน/พาร์เชียลฟอสฟอริเลตพอลิไวนิลแอลกอฮอล์เอนแคปซูเลตด้วยพอลิอะคริเลต ผ่านวิธีซีดอิมัลชันพอลิเมอไรเซชันแบบปราศจากอิมัล-ซิฟายเออร์ (PAn/P-PVA)/PAc อนุภาคนาโนถูกเตรียมขึ้นโดยเปลี่ยนแปลงปริมาณอะคริเลต 4, 6 และ 8 กรัม พบว่ามีค่าการเปลี่ยนแปลงมอนอเมอร์สูงสุดที่ร้อยละ 93.9 ที่ปริมาณพอลิแอนิลีน/พาร์-เชียลฟอสฟอริเลตพอลิไวนิลแอลกอฮอล์และปริมาณอะคริเลตที่เหมาะสม จากการพิสูจน์เอกลักษณ์ด้วยเครื่องเอ็กซเรย์ดิฟแฟรคโตมิเตอร์ พบว่าพอลิอะคริเลตแทรกสอดระหว่างชั้นของ PAn/P-PVA ฟูเรียทรานฟอร์มอินฟราเรดสเปคโตรสโคปีของ (PAn/P-PVA)/PAc แสดงหมู่ฟังก์ชันไฮดรอกซิล (-OH), คาร์บอกซิล (C=O), ฟอสโฟไดเอสเตอร์ (P=O) และ วงเบนซีนอยด์ จากสัณฐานวิทยาของนาโนพาร์ติเคิลโดยกล้องจุลทรรศน์อิเล็กตรอนแบบส่องกราดและแบบส่องผ่าน พบว่าอนุภาค PAn/P-PVA มีลักษณะเป็นทรงกลมเกาะกลุ่ม และถูกเคลือบด้วยพอลิอะคริเลต จากการวิเคราะห์สมบัติเชิงความร้อน พบว่า (PAn/P-PVA)/PAc นาโนพาร์ติเคิลมีเสถียรภาพเชิงความร้อนที่ต่ำลง เมื่อเพิ่มปริมาณอะคริเลต ในด้านของไฟฟ้าเคมี ใช้วิธีการวัดไซคลิกโวลแทมเมตรีโดยนำ (PAn/P-PVA)/PAc เคลือบบนผ้าคาร์บอนไฟเบอร์อนุภาคนาโน PAn/P-PVA ที่แอนแคปซูเลตด้วย PAc ที่มีสมบัติเป็นฉนวนไฟฟ้า และพบว่าเมื่อเพิ่มปริมาณอะคริเลตมากขึ้นทำให้พีคของค่าการนำไฟฟ้าผ่านไซคลิกโวลแทมเมตรีลดลง จากการศึกษาการกัดกร่อน ในสารละลายกรดซัลฟิวริก ความเข้มข้น 1.0 โมลาร์ พบว่าเหล็กกล้าเคลือบด้วย (PAn/P-PVA)/PAc-8c นาโนคอมพอสิตแสดงค่าความต้านทานการกัดกร่อนในดีที่สุดร้อยละ 11.4 เมื่อเพิ่มปริมาณอะคริเลตในนาโนคอมพอสิตสามารถปรับปรุงสมบัติของการป้องกันการกัดกร่อน เนื่องจากเพิ่มความคดเคี้ยวของทางเดินการซึมผ่านของสารกัดกร่อน

สาขาวิชา ปิโตรเคมีและวิทยาศาสตร์พอลิเมอร์ ลายมือชื่อนิสิต……..……

ปีการศึกษา 2556 ลายมือชื่อ อ.ที่ปรึกษาวิทยานิพนธ์หลัก…...……....

ลายมือชื่อ อ.ที่ปรึกษาวิทยานิพนธ์ร่วม…...……....

5472046523: MAJOR PETROCHEMISTRY AND POLYMER SCIENCE
KEYWORDS: POLYANILINE/ EMULSION POLYMERIZATION/ ENCAPSULATION/ CONDUCTING POLYMER

PHANRAPEE VARAKIRKKULCHAI: CONDUCTING POLYANILINE NANOPARTICLES ENCAPSULATED WITH POLYACRYLATE VIA EMULSIFIER FREE SEEDED EMULSION POLYMERIZATION. ADVISOR: PROF. PATTARAPAN PRASASSARAKICH, Ph.D., CO-ADVISOR: SUWADEE KONGPARAKUL, Ph.D., 86 pp.

Polyaniline/partially phosphorylated poly(vinyl alcohol)/polyacrylate (PAn/P-PVA)/PAc nanoparticles were synthesized by encapsulation of PAn/P-PVA nanoparticles with PAc via the emulsifier-free seeded emulsion polymerization. The (PAn/P-PVA)/PAc nanoparticles were prepared by varying acrylate amounts. The results showed that the maximum monomer conversion was 93.9% at appropriate loading of (PAn/P-PVA) nanoparticles and acrylate monomers. From X-ray diffraction analysis, the results showed that PAc were intercalated between the PAn/P-PVA layer. Fourier-transform infrared spectroscopy (FT-IR) spectra of (PAn/P-PVA)/PAc showed the functional groups of hydroxyl (-OH), carboxyl (C=O), phosphodiester (P=O) and benzenoid ring. The nanoparticles morphology were observed by scanning electron microscope (SEM) and transmission electron microscope (TEM). The spherical PAn/P-PVA agglomerates were coated with PAc. From thermogravimetric analysis, stability of (PAn/P-PVA)/PAc nanoparticles was decreased with increasing acrylate amount. For electrochemical aspect, the (PAn/P-PVA)/PAc coated on carbon fiber electrode was subjected to cyclic voltammetry (CV). The PAn/P-PVA nanoparticles were encapsulated sufficiently by the non-conductive PAc and it was found that as the acrylate amount increased, the peak current observed during CV decreased. From corrosion study in 1.0 M sulfuric acid solution, steel coated with (PAn/P-PVA)/PAc-8c nanocomposites showed the best corrosion resistance (CR) of 11.4%. The increase in the acrylate amount in nanocomposites improve the anticorrosive properties due to an increasing tortuosity of diffusion pathway of corrosion agents.

Field of Study: Petrochemistry and Polymer Science Student's Signature……

Academic Year: 2013 Advisor's Signature……...

Co-advisor's Signature…….

ACKNOWLEDGEMENTS

The author would like to express her gratitude to her supervisors, Prof. Dr. Pattarapan Prasassarakich and co-advisor, Dr.Suwadee Kongparakul (Department of Chemistry, Faculty of Science and Technology, Thammasat University) for her encouraging guidance, supervision and helpful suggestion throughout her research. The author also would like to acknowledge Prof. Dr. Tharapong Vitidsant, Assoc. Prof. Dr. Nuanphun Chantarasiri, and Assoc. Prof. Dr. Ittipol Jangchud for their participation on the dissertation chairman and members of thesis committee, respectively.

The author would like to gratefully acknowledge Asst. Prof. Dr. Nisit Tantavichet for his helpful suggestion throughout her research, Program of Petrochemistry and Polymer Science, Department of Chemical Technology, Faculty of Science, Chulalongkorn University.

A warm thank is expressed to all of her friends in the laboratory for their friendships and help during the course of her research.

Finally, and most of all, the author would like to express her deep appreciate to her family for their love, support and endless encouragement throughout her entire study.

CONTENTS

Page

Page

Page

LIST OF TABLES

LIST OF FIGURES

Figure **Page**

Figure **Page**

Figure **Page**

LIST OF ABBREVIATIONS

AA	:	Acrylic acid
APS	:	Ammonium persulfate
BA	:	Butyl acrylate
CR	:	Corrosion rate
CV	:	Cyclic voltammogram
$\overline{D}_n$	:	Mean number diameter (average particle size)
E_{corr}	:	Corrosion potential
EGDMA	:	Ethylene glycol dimethacrylate
FTIR	:	Fourier transform infrared spectroscopy
I_{corr}	:	Corrosion current
MMA	:	Methyl methacrylate
PAc	:	Polyacrylate
PAn	:	Polyaniline
PAn/P-PVA	:	Polyaniline/partially phosphorylated poly(vinyl alcohol)
(PAn/P-PVA)/PAc	:	Polyaniline/partially phosphorylated poly (vinyl-alcohol)/polyacrylate
P-PVA	:	Partially phosphorylated poly(vinyl alcohol)
PSD	:	Particle size distribution
SEM	:	Scanning electron microscopy
TEM	:	Transmission electron microscopy
TGA	:	Thermogravimatric analysis
XRD	:	X-Ray diffraction

CHAPTER I

INTRODUCTION

1.1 The Purpose of the Investigation

With the discovery in 1960 of intrinsically conducting polymers (ICPs), an attractive subject of research was initiated because of the interesting properties and numerous application possibilities of ICPs. It was expected that ICPs would find their potential applications such as electrical, electronics, electrochemical, electromagnetic and chemical [1]. Electrically conducting organic polymers are a novel class of 'synthetic metals' that combine the chemical and mechanical properties of polymers with the electronic properties of metals and semiconductors. These polymers become conductive upon partial oxidation or reduction, a process referred to as doping. It has been demonstrated that the electrical properties of conductive polymers can be reversibly changed over the full range from an insulator to a metallic conductor.

Polyaniline (PAn) is one of the most important conducting polymers due to its excellent electrical conductivity, electrochemical properties, good environmental stability, low cost and facile synthesis. It also has potential application in many fields, such as electrodes, electromagnetic shielding materials, anticorrosion coating, sensor devices and catalysts. However, there are some potential applications of PAn which have not been exploited, such as poor processability and least anticorrosive properties, an effective method that can solve the processability of PAn is to prepare the composites of PAn with easily processable polymers. Dispersion of PAn can be prepared by dispersion and emulsion polymerization using an appropriate stabilizer and surfactant, respectively [2]. Moreover, some types of the stabilizer and surfactant can act as dopant as well. And the core-shell composites with PAn as shell and polyacrylate as core materials are usually synthesized, allowing the fabrication of the PAn composites improve the mechanical strength, thermal stability, fire retardant and anticorrosive properties [3]. Therefore, the addition of polyacrylate into PAn could improve the processability and mechanical properties.

In this research work, the P-PVA, a phosphoric ester, prepared by the phosphorylation of PVA with phosphoric acid. The P-PVA was used as a stabilizer and codopant for the colloidal PAn dispersion. The colloidal PAn dispersion was prepared by the chemical oxidative polymerization of aniline in HCl aqueous solution with APS as an oxidant. The conducting polyaniline/partially phosphorylated poly(vinyl alcohol)/polyacrylate ((PAn/P-PVA)/PAc) nanoparticles were prepared by the encapsulation of PAn/P-PVA with polyacrylate (PAc) via the emulsifier-free seeded emulsion polymerization. The PAn/P-PVA nanoparticles were synthesized by *in situ* chemical oxidative polymerization. The electroactivity and anticorrosive properties of polyaniline/partially phosphorylated poly(vinyl alcohol)/polyacrylate ((PAn/P-PVA)/PAc) nanocomposites were investigated.

1.2 The Objectives

The objectives of thesis can be summarized as follows:

1. To prepare the PAn/P-PVA by *in situ* chemical oxidation polymerization and encapsulate PAn/P-PVA with polyacrylate via emulsifier-free seeded emulsion polymerization.
2. To study the thermal properties and morphology of (PAn/P-PVA)/PAc nanoparticles.
3. To study the conducting and anti-corrosion properties of (PAn/P-PVA)/PAc nanocomposites.

1.3 Scope of the Investigation

The experimental procedure for this research was presented as follows:

1. Literature survey and in-depth study for this research work.
2. Prepare the PAn/P-PVA by *in situ* chemical oxidation polymerization
3. Prepare the (PAn/P-PVA)/PAc by encapsulation with polyacrylate (PAc) via emulsifier-free seeded emulsion polymerization and study the effects of acrylate amount at 4, 6 and 8 g.

4. Investigate the monomer conversion, particles size and solid content for preparation of PAn/P-PVA and (PAn/P-PVA)/PAc nanoparticles.
5. Characterize the PAn/P-PVA and (PAn/P-PVA)/PAc nanoparticles by Fourier transform infrared spectroscopy and X-ray diffraction analysis.
6. Investigate the thermal properties and morphology of PAn/P-PVA and (PAn/P-PVA)/PAc nanoparticles.
7. Investigate electroactivity and anti-corrosion performance of (PAn/P-PVA)/PAc nanocomposites.
8. Analyze data and summarize the results.

CHAPTER II

THEORY AND LITERATURE REVIEW

Intrinsically Conducting Polymers (ICPs) is one of attractive materials because of the interesting properties and numerous applications of ICPs. It was expected that ICPs would find their potential applications in multidisciplinary areas such as electrical, electronics, thermoelectric, electrochemical, electromagnetic, electromechanical, electro-luminescence, electro-rheological, chemical, membrane, and sensors

2.1 Electrically Active Polymers and Composites [4]

Generally, there are four primary types of electrically active polymer system with different degrees of conductivities.

1. The most widely used conducting polymeric systems are the composites in which an insulating polymer matrix is filled with a particulate or fibrous conductive fillers such as a carbon or a metal to impart high conductivity. Applications for such composites are widely used such as interconnections, printed circuit boards, encapsulations, die attach, heat sinks, conducting adhesives, electromagnetic interference (EMI) shielding, electrostatic discharge (ESD), and aerospace engineering.

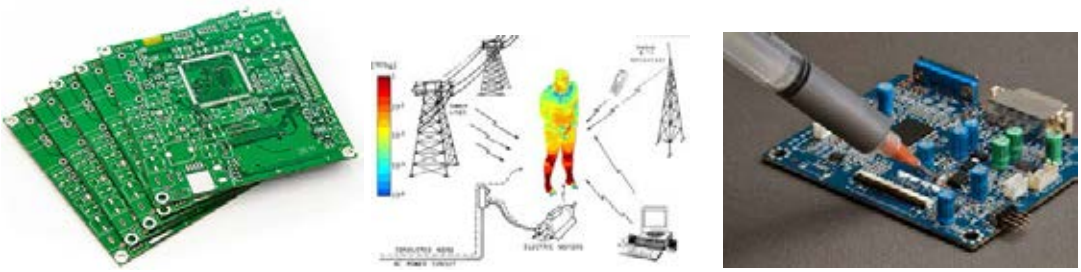

(a) (b) (c)

Figure 2.1 (a) printed circuit boards, (b) electromagnetic interference (EMI) shielding and (c) conducting adhesives [5]

2. The polymer is known as ionically conducting polymers. Here, the origin of electrical conductivity is a result of the movement of ions presented in the system. An example of such a polymer is polyethylene oxide, in which lithium ions are mobile. These types of polymers are applied in the battery industry.

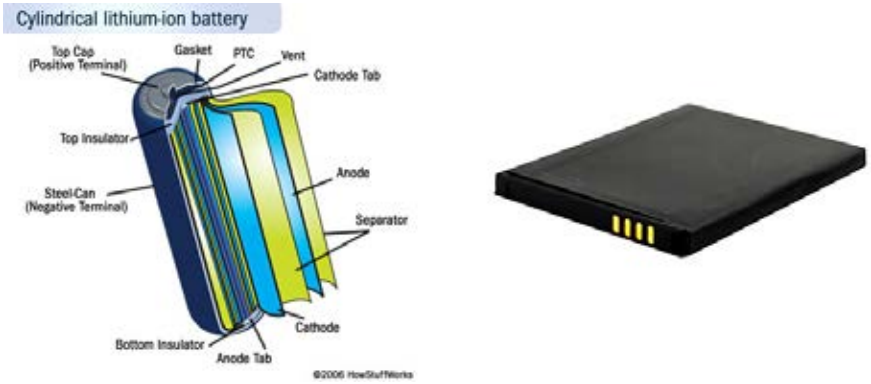

(a) (b)

Figure 2.2 (a) lithium-ion and (b) battery of mobile [6]

3. The last group of conducting system is conjugated polymers. These polymers consist of alternating single and double bonds, creating an extended π network. The movement of electrons within this π framework is the source of conductivity. However, dopant is required to increase the level of conductivity for this type of polymers.

2.1.1 Intrinsically Conducting Polymers (ICPs) [7]

ICPs are inherently conducting polymers in nature due to the presence of a conjugated π electron system in their structure. ICPs have a low energy optical transition, low ionization potential and a high electron affinity. A high level of conductivity (near metallic) can be achieved in ICPs through oxidation-reduction as well as doping with a suitable dopant. Following the study on polyacetylene, other polymers such as polypyrrole (PPY), polythiophene, polyaniline, poly (*p*-phenylenevinylene), and poly (*p*-phenylene), as well as their derivatives, have been synthesized and reported as a new group of polymers known as ICPs. The structures of a few intrinsically ICPs are shown in Figure 2.3. The conductivity of a number of ICPs relative to copper and liquid mercury is presented in Figure 2.4.

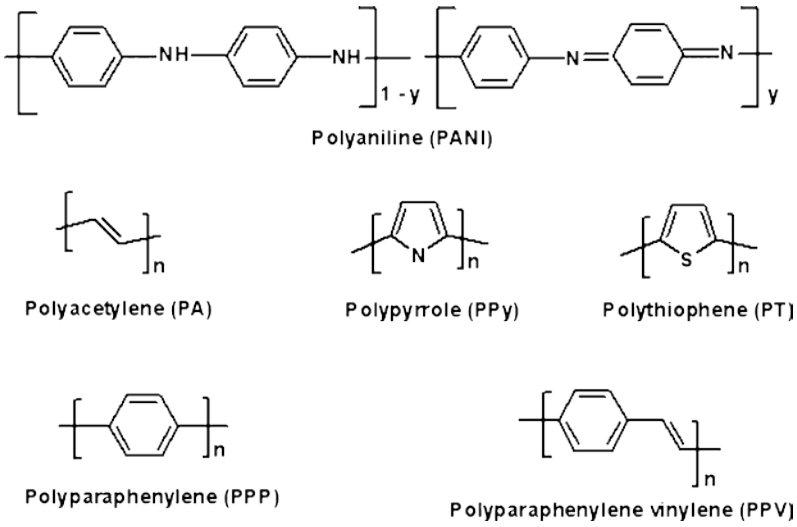

Figure 2.3 The structure of a number of intrinsically conducting polymers (ICPs) [7]

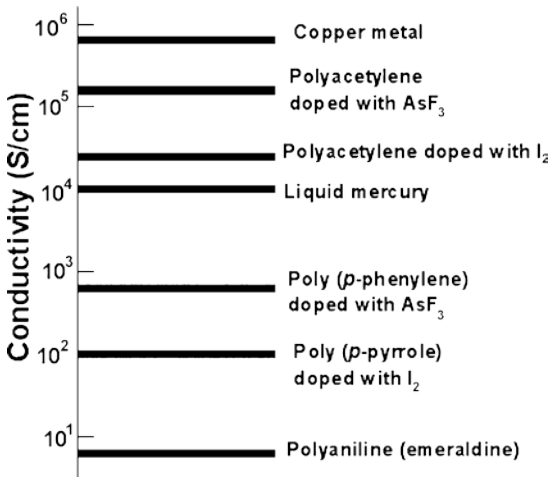

Figure 2.4 The conductivity of a number of ICPs relative to copper and liquid mercury [7]

2.1.2 Superiority of Polyaniline Compared to Other ICPs [7]

The thermal stability of PAn is superior to other ICPs. The processability and conductivity of PAn are also fairly good. From economic point of view, PAn is significantly superior to other ICPs because the aniline monomer is less expensive than other monomers used for ICP. The synthesis of PAn is very simple, properties can be tuned easily, and it has numerous application possibilities. All these factors contribute to PAn being superior to other ICPs.

2.2 Polyaniline [8]

The polyaniline (PAn) is one of the conductive polymers. PAn and its derivatives have been widely used in various fields, due to their easily in synthesis process, electrical conductivity, chemical or electrochemical redox reversibility, good environmental stability and cheapness. The important structure of PAn family is the π-conjugated system and aromatic ring containing the nitrogen atom. Due to the reversible redox and pH-switching properties, PAn has been the most extensively studies in the conductive organic polymers. PAn and its derivatives have commonly synthesized through the chemical polymerization and electrochemical polymerization. Based on their advantages, PAn and its derivatives have been currently being developed and used in a wide range of potential applications including science and

technology, such as anticorrosion coating, batteries, sensor devices, electrochromic devices and coating for metallic surfaces.

Polyaniline refers to a class of polymers which can be considered as being derived from a repeating unit, the base form of which has the generalized composition (Figure 2.5) and which consists of alternating reduced and oxidized repeating units. In each repeating unit, there are three benzene rings separated by amine (−NH) groups and one quinoid ring surrounded by imine (−N=) groups. For the quinoid ring which forms double bonds with the nitrogens, there are two pairs of carbon atoms in the ring and four π-electrons. The macroscopic structure of the polymer is made up of many long chains of repeat units forming a complicated network.

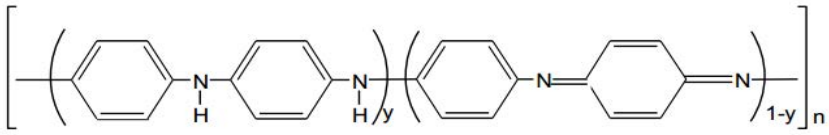

Reduced repeating units Oxidized repeating units

Figure 2.5 The basic geometrical structure of polyaniline [7]

Generally polyaniline exists in three forms depending on the oxidation state namely Leucoemaraldine (y=1), Permigraniline (y=0) and Emaraldine (y=0.5) that differ in chemical and physical properties as presented in Table 2.1. In the Emaraldine form, it exists in insulating state [Emaraldine base (EB)] and conducting state [Emaraldine salt (ES)]. Emaraldine salt form is obtained upon protonation of Emaraldine base with protonic acids i.e., oxidative doping. The fundamental properties of polyaniline depend on the mechanism of charge transfer in the polymer as shown in Figure 2.6. [9].

Table 2.1 The different forms of polyaniline [8].

Form	Name	Color	Conductivity(S/cm)
Fully reduced form	Leucoemeraldine base (LEB)	Yellow, White/clear	$< 10^{-5}$
Partially reduced form	Emeraldine base (EB)	Blue	$< 10^{-5}$
Fully oxidized form	Pernigraniline (PNB)	Purple	$< 10^{-5}$
	Emeraldine salt (ES)	Green	~15

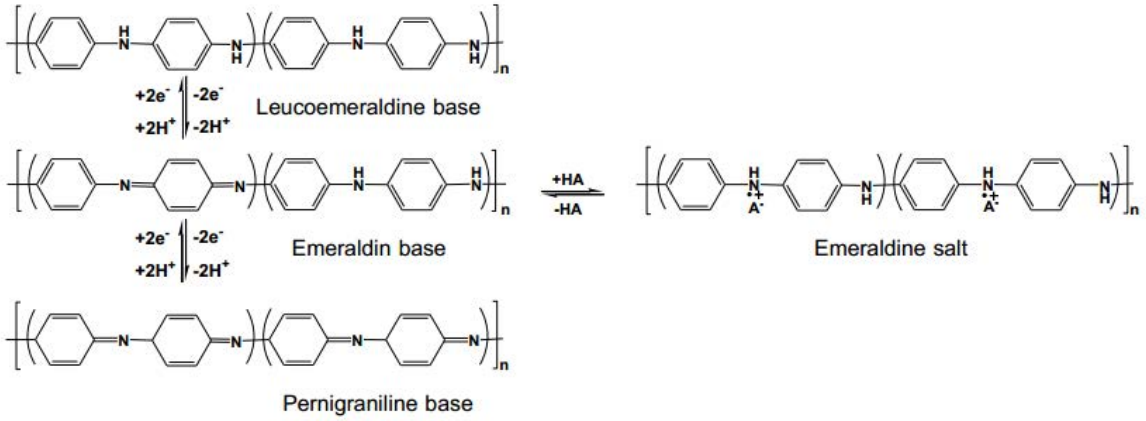

Figure 2.6 Doping mechanisms of PAn [7]

Polyaniline is a typical phenylene-base polymer having a chemically flexible –NH– group in a polymer chain flanked either side by phenylene ring. The protonation, deprotonation and several other physico-chemical properties of polyaniline could be carried on due to the presence of the –NH– group. Conductivity of polyemeraldine base is around 10 S/cm. Polyaniline is found to be the most useful because of good environmental stability, conductivity and low cost.

2.2.1 The Reaction Mechanism of Polyaniline [7]

The reaction mechanism of aniline polymerization is shown in Figure 2.7. First step is the aniline monomer from anilinium ion in acidic medium and chemical polymerization result in the formation of protonated, partially oxidized form of polyaniline. This step involves aniline forming radical cation. The second step is the coupling of –N– in amine functional group and para-radical cation with consecutive re-aromatization of the di-cation. The final step is the oxidation process of the di-radical di-cation makes the fully oxidized pernigraniline salt form of polyaniline due to the high oxidizing power of oxidant; the oxidant used in the experiment was ammonium persulfate (APS). This would create head to tail coupling in the ortho-position also occurs resulting in a conjugation defect in the final product.

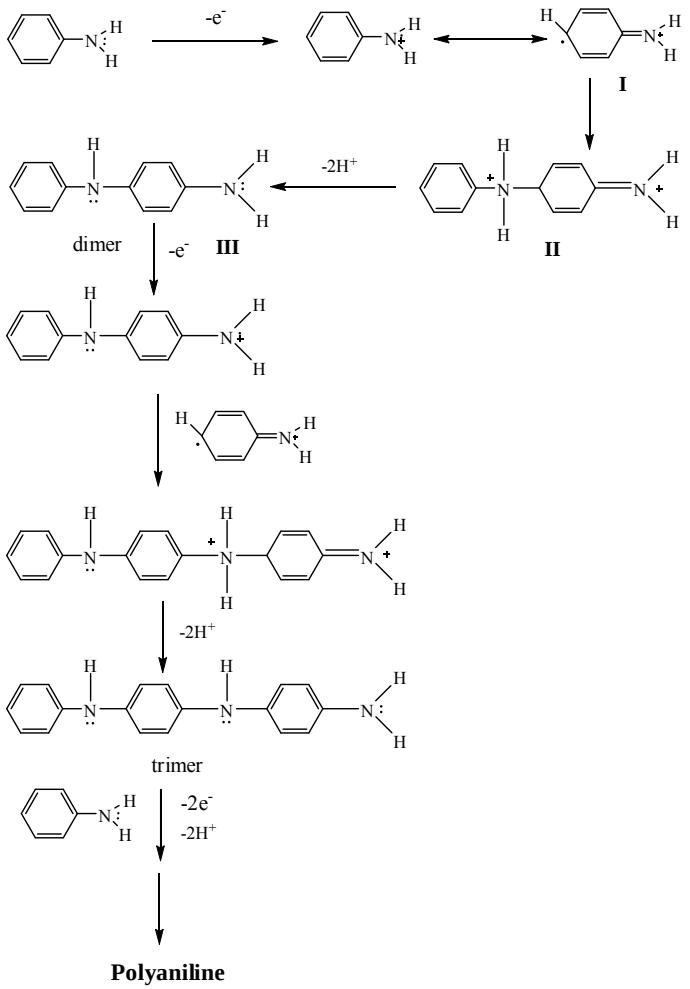

Figure 2.7 Reaction mechanism of aniline polymerization [8]

2.3 Phosphorylation of PVA (P-PVA) [10, 11]

Partially phosphorylated poly(vinyl alcohol) (P-PVA) has attracted considerable interest because of its nonflammability, metal complexes, anionic polyelectrolyte hydrogels, and cation exchange resins. The Partially phosphorylated poly (vinyl alcohol) is a phosphoric ester prepared via crosslink reaction by the phosphorylation of PVA with phosphoric acid in an aqueous media. The P-PVA was used as the stabilizer and co-dopant for the colloidal PAn dispersion. The synthesis route of P-PVA is shown in Figure 2.8.

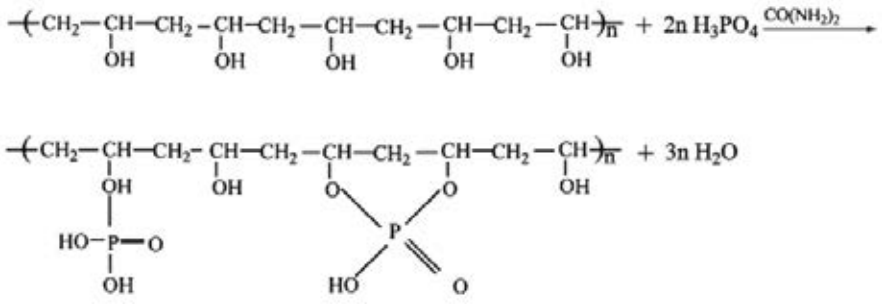

Figure 2.8 Synthesis route to partially phosphorylated poly(vinyl alcohol) (P-PVA) [12]

2.4 Encapsulation of Polyaniline Nanoparticles [13]

Emulsifier-free (or soapless) emulsion polymerization is a technique derived from conventional emulsion polymerization in which polymerization is carried out in the absence of emulsifiers as shown in Figure 2.9. This technique has been extraordinarily useful for the preparation of model polymer colloids with narrow particle size distributions, green process and well characterized surface properties. Emulsifier-free emulsion polymerization eliminates the disadvantages of conventional emulsion polymerizations stemming from the use of emulsifiers, e.g. impurities in products caused by unremoved emulsifier and poor water-resistance of films formed by polymer latex. Although emulsifier-free emulsion polymerization is a kind of emulsion polymerization without added emulsifier, the system gains colloidal stability via the involvement of one of the following reactive components which acts as an emulsifier: (1) ionizable initiator (2) hydrophilic co-monomers (3) ionic co-monomers.

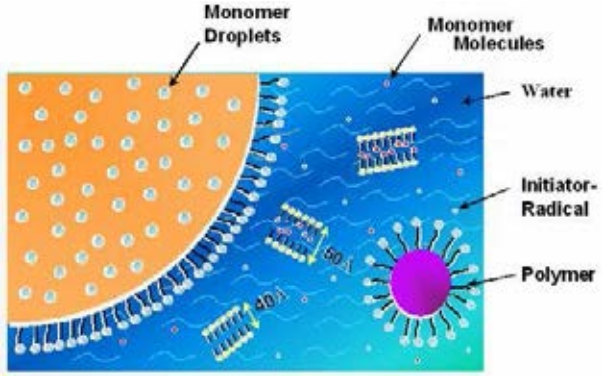

Figure 2.9 Emulsifier-free emulsion polymerization [14]

The encapsulation of the PAn/P-PVA nanoparticles was accomplished by the emulsifier-free seeded emulsion polymerization and straved-free technology of acrylate monomer. Emulsifier-free seeded emulsion polymerization technique was used to encapsulate the PAn/P-PVA nanoparticles as a core within polyacrylate (PAc) as a shell as shown in Figure 2.10.

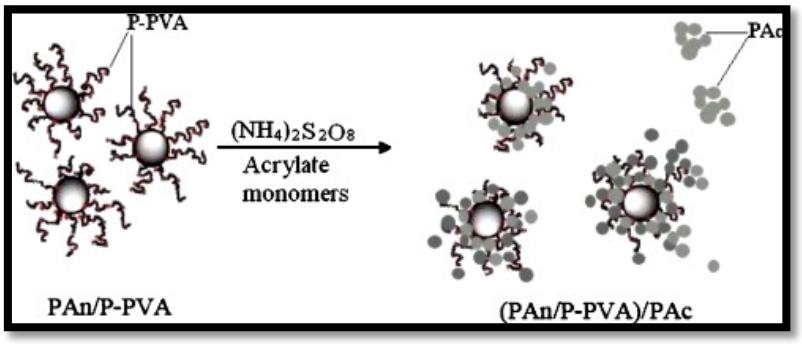

Figure 2.10 PAn/P-PVA nanoparticles encapsulated with PAc latex [15]

2.5 Electrical of Electrically Conducting Polymer (ECPs) [16]

Conducting polymers (CPs) are extensively conjugated molecules contain alternating single and double bonds. In these molecules, electrons are able to move from one end of the polymer to the other through the extended *p*-orbital system. Hence CPs is known to be either semiconductors or conductors, which are related to how bands and shells of electrons form within a compound. In view of an electronics of electrically conducting polymers (ECPs), the band theory is employed to explain the mechanisms of conduction in CPs.

2.5.1 The Band Theory [16]

The energy band that results from the bonding orbitals of a molecule is known as the valence band, while the conduction band is as a result of the antibonding orbitals of the molecule as illustrated in Figure 2.11. The width of individual bands across the range of energy levels is called band width. The highest occupied molecular orbital (HOMO) is represented by the valence band (VB) and the lowest unoccupied molecular orbital (LUMO**)** is represented by the conduction band (CB). The gap between the highest filled energy level and lowest unfilled energy level is called band gap (Eg). A range of energies are represented by the band gap which is not available to electrons transfer and this gap is known variously as 'the fundamental energy gap', the 'band gap', the 'energy gap', or the 'forbidden gap'. The level of electrons in a system which is reached at absolute zero is called the Fermi level (Fg). It has been demonstrated that in order to allow the formation of delocalized electronic states, CPs molecular arrangement must be conjugated. The size of the energy band gap depends on extend of delocalization and the alternation of double and single bonds. Furthermore, the size of the energy band gap will determine whether CP is metal, semiconductor or insulator. In the atomic and molecular orbital theory are explained by combining the concepts, the electronic properties of metals, semiconductors, and insulators can be differentiated with reference to the energy band gap as shown in Figure 2.11.

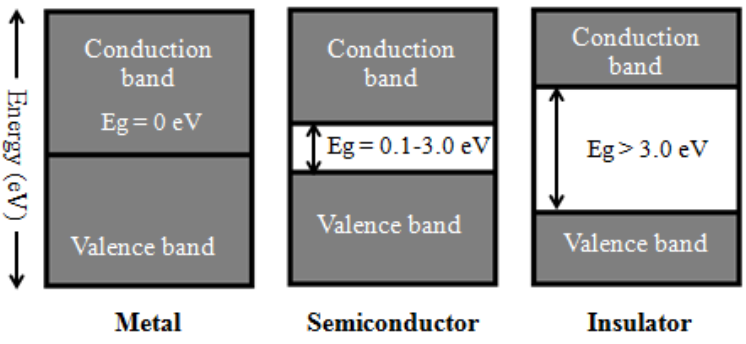

Figure 2.11 Energy band gaps diagram [16]

2.5.2 The Electronic Properties of Semiconductors [16]

There are two possible scenarios which can allow a material to become a conductor. The first instance is when the VB is not completely filled, thus an electron can raise its energy to a higher level within the valence band, so that it can detach from its atom. This is coined as conduction within same band, and it requires a small amount of energy, hence many electrons are capable of accomplishing it. Second instance is when the band gap is very small, hence electrons can raise their energy and detach from their atoms by jumping to a higher energy level in the CB. Once these electrons have reached the conduction band, they contribute to the electrical conductivity. Moreover, the holes which are created in the valence band, by the electrons jumping to the conduction band, also contribute to electrical conductivity.

2.5.3 Electrical Conduction in Polyaniline [7]

The electrical conductivity (σ) in any system is proportional to the product of the density of charge carriers (e) the charge carried by each carrier (n) and the mobility of each carrier (μ).

$$\sigma = en\mu \qquad (2.1)$$

Here e is the unit electronic charge ($1.6\times^{10-19}$ C), 'n' in m^{-3} and μ in m^2/ (V s).

The carrier concentration, its mobility and the type of carrier of semiconductors, can be estimated from a Hall effect measurement. The experimental results show that the majority charge carriers in PAn are holes, which indicates that the PAn is a *p*-type semiconductor. The delocalized π bonds available in the system are responsible for the semi-conducting properties. The value of this band gap determines both the electrical and optical properties of semi-conducting polymers. As the band gap energy decreases, the π-π* transition becomes easier, resulting in a high conductivity.

PAn is a semi-crystalline, heterogeneous system with a crystalline (ordered) region dispersed in an amorphous (disordered) region as shown in Figure 2.12. The crystalline domains are metallic in nature, where conduction occurs through electron delocalization or hopping of the charge carrier due to the ordered structure. The conduction in the metallic region occurs by the hopping of charge carrier through the polaron structure.

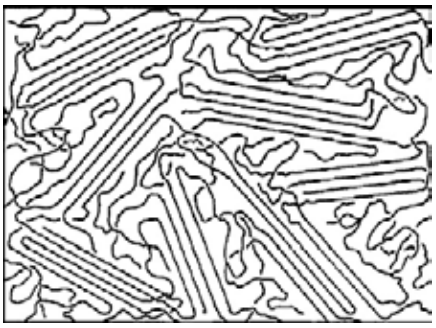

Figure 2.12 Crystalline (ordered)-amorphous (disorder) or heterogeneous structure of Polyaniline [7]

2.5.4 Conductivity Properties of Polyaniline [16]

It has been previously demonstrated that the polyaniline chain can be formed by various combinations of the two repeating units known as the X and Y components of polyaniline. Owing to this, PAn has many unique properties and electronic conduction mechanisms that distinguish it from the rest of the conducting polymers. Among the various oxidation states that PAn can exist in, the one that can be doped to a highly conductive state is the moderately oxidized emeraldine base. This form of PAn has a structure which consists of equal proportions of amines (–NH–) and imine (=N–) sites. Through protonic acid doping, imine sites are protonated by acid HA to the bipolaron (dication salt) form. The bipolaron then undergoes a further rearrangement to form the delocalized polaron lattice which is a polysemiquinone radical-cation salt as shown in Figure 2.13.

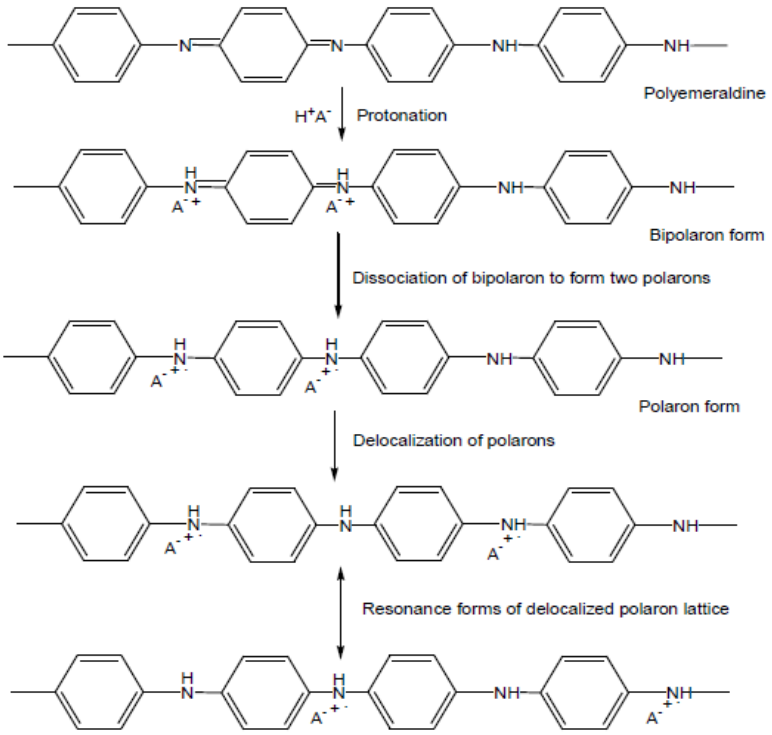

Figure 2.13 The doping of EB with protons to form the conducting emeraldine salt (PAn/HA) form of polyaniline (a polaron lattice) [16]

In the polaron structure, a cation radical of one nitrogen were acted as the hole and these holes are charge carrier. The electron from the adjacent nitrogen (neutral) jumps to that hole (right hand side of Figure 2.14) and that hole then becomes neutral. Consequently, the holes start to move (left hand side of Figure 2.14) as schematically presented in Figure 2.14. As a result, on the second nitrogen another hole is created. Hence, in the polaron structure an electron starts moving along the polymer chain towards one particular direction (to the right of Figure 2.14) and the corresponding hole are set into motion along the chain length in the opposite direction (to the left of Figure 2.14) leading to an electrical conduction along the chain.

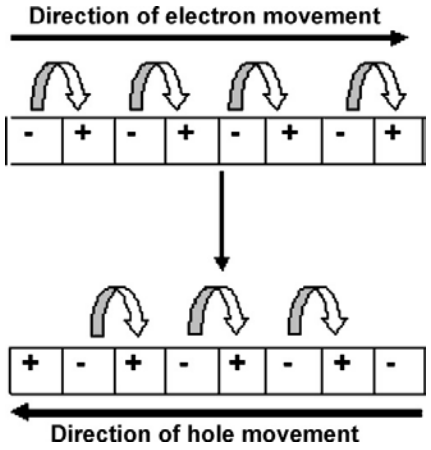

Figure 2.14 Schematic presentation of conduction pathway of polyaniline (the +ve sign represent the cation redical acting as a hole and the –ve sign represents neutral nitrogen) [7]

2.6 Electrochemistry [17, 18]

Electrochemistry is a chemical reactions which take place in a solution at the interface of an electron conductor (the electrode: a semiconductor or a metal) and an ionic conductor (the electrolyte). These reactions associate electron transfer between the electrode and the electrolyte or species in solution.

If a chemical reaction is driven by an externally applied voltage, as in electrolysis, or if a voltage is created by a chemical reaction as in a battery, it is an *electrochemical* reaction. In contrast, chemical reactions where electrons are transferred between molecules are called redox (oxidation-reduction) reactions. In general, electrochemistry deals with situations where redox reactions are separated in space or time, connected by an external electric circuit. Two electrodes are consisted of electrochemical cells: an anode (the electrode at which the oxidation reaction occurs) and a cathode (the electrode at which the reduction reaction occurs).

The cell (E°_{cell}) potential at standard conditions can be found through this equation:

$$E^{\circ}_{cell} = E^{\circ}_{cathode} - E^{\circ}_{anode} \quad (2.2)$$

Because cell potential is based on the potential energy per unit of charge, it is an intensive property.

2.6.1 Composition of electrochemical cells

Electrodes used in Electrochemistry

To perform such an experiment requires at least two electrodes, the working electrode, which makes contact with the analyte, must apply the desired potential in a controlled way and facilitate the transfer of charge to and from the analyte. A second electrode acts as the other half of the cell. This second electrode must have a known potential which use to measure the potential of the working electrode, moreover it must balance the charge added or removed by the working electrode. While this is available setup, it has a number of shortcomings. Most significantly, it is exceedingly difficult for an electrode to maintain a constant potential while passing current to counter redox events at the working electrode [Figure 2.15].

- **The working electrode, WE** is an electrode in the electrochemical system on which the reaction of interest is occurring. It is usually made of inert materials e.g. Au, Ag, Pt, glassy carbon (GC), carbon fiber cloth and Hg drop and film electrodes. For corrosion applications, the material of the working electrode is the material under investigation (which is actually corroding). The size and shape of the working electrode also varies and it depends on the application.
- **The counter electrode, CE** (also known as auxiliary electrode), is an electrode which is used to close the current circuit in the electrochemical cell. It is usually made of an inert material (e.g. Pt, Au, graphite, glassy carbon) and usually it does not participate in the electrochemical reaction. Because the

current is flowing between the WE and the CE, the total surface area of the CE (source/sink of electrons) must be higher than the area of the WE so that it will not be a limiting factor in the kinetics of the electrochemical process under investigation.

- **The reference electrode, RE** is an electrode which has a stable and well-known electrode potential and it is used as a point of reference in the electrochemical cell for the potential control and measurement. The high stability of the reference electrode potential is usually reached by employing a redox system with constant (buffered or saturated) concentrations of each participants of the redox reaction. Furthermore, the current flow through the reference electrode is kept close to zero (ideally, zero) which is achieved by using the CE to close the current circuit in the cell together with a very high input impedance on the electrometer.

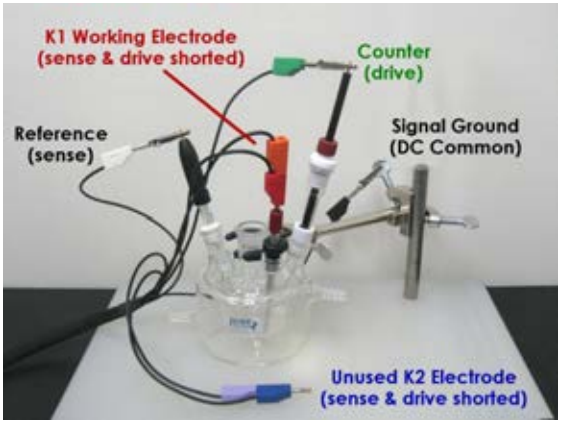

Figure 2.15 Electrode configuration of electrolytic cell [19]

Electrolyte

An electrolyte is a compound that ionizes when dissolved in suitable ionizing solvents e.g. water. This includes most soluble salts, acids, and bases. Some gases, e.g. hydrogen chloride, under conditions of high temperature or low pressure can also function as electrolytes. Electrolyte solutions are generally formed when a salt is placed into a solvent such as water and the individual components dissociate

due to the thermodynamic interactions between solvent and solute molecules, in a process called solvation.

1. Generator

A generator produces an electric current by electromagnetic induction. A generator does not produce electrons - it pumps electrons toward the cathode and away from the anode. The role of a generator is to raise the potential energy of the electrons on the cathode and to reduce the potential energy of the electrons on the anode.

The most common experimental techniques used for study of electrochemical properties of materials:

1. Potentiostatic technique

The potentiostatic is a control and measuring device for an electrolytic cell, that keeps the potential of the working electrode at a constant level respect to the reference electrode [1]. It consists of an electric circuit which controls the potential across the cell by sensing changes in its resistance, varying accordingly the current supplied to the system: a higher resistance will result in a decreased current, while a lower resistance will result in an increased current, in order to keep the voltage constant. Important features of potentiostatic deposition are:

i) Controls the potential of working electrode with respect to reference electrode.
ii) The potential at counter electrode is driven to the required potential to establish the desired working electrode potential.
iii) The output waveform gives the variation of cell current with time.

2. Galvanostatic technique

Three electrode configurations are used by the glavanostatic, in which a current is applied between the auxiliary and working electrodes and monitored the potential of the working electrode (measured with respect to the reference electrode). The basis of controlled current experiments is that a redox (electron transfer) reaction must occur at the surface of the working electrode in order to support the applied current. A

constant current stripping potentiometry and constant current electrolysis are included common applications of the galvanostatic (including applications where a constant rate of electrolysis is important, such as electrodeposition and battery studies). Important features of galvanostatic deposition are:

i) It controls the current between counter electrode and working electrode at selected current range.

ii) The counter electrode is driven to the potential required to establish the desired cell current.

iii) Reference electrode is not used for controlling current but it is used to measure potential at some point in electrochemical cell.

iv) The output waveform gives the variation of cell potential with time.

3. Cyclic voltammetry technique [17, 19]

This technique is used as an electrochemical analytical as well as varying potential electrodeposition technique. Cyclic voltammetry [Figure 2.16] or potentiodynamic is a method in which electrolysis currents are measured as a function of imposed potential. This technique is a tool for studying the various electrochemical processes taking place during electrolysis such as charge transfer and electrode kinetics. It gives qualitative information of electrochemical reaction. By studying cyclic voltammogram from an electrochemical hysteresis redox potential of an electroactive species in the solution can be determined. In this technique, electrochemical process taking place entirely in the solution phase, a new solid phase is formed on the substrate surface due to the redox state. Important features of cyclic voltammetry deposition are:

i) Measures the current during triangular potential sweep and observes both the anodic and cathodic responses.

ii) The output waveform has both forward and reverse peaks that give information about the electroactivity of electrode or the solution.

In typical cyclic voltammetry, a solution component is electrolyzed (reduced or oxidized) by placing the solution in contact with the electrode surface, and then making that surface sufficiently positive or negative in voltage to force electron

transfer. In simple cases, the surface is started at a particular voltage with respect to a reference half-cell such as calomel or Ag/AgCl, the electrode voltage is changed to a higher or lower voltage at a linear rate, and lastly, the voltage is changed back to the original value at the same linear rate. When the surface becomes sufficiently negative or positive, a solution species may gain electrons from the surface or transfer electrons to the surface. This results in a measurable current in the electrode circuitry. However, if the solution is not mixed, the concentration of transferring species near the surface drops, and the electrolysis current then falls off. When the voltage cyclic is reversed, it is often the case that electron transfer between electrode and chemical species will also be reversed, leading to an "inverse" current peak.

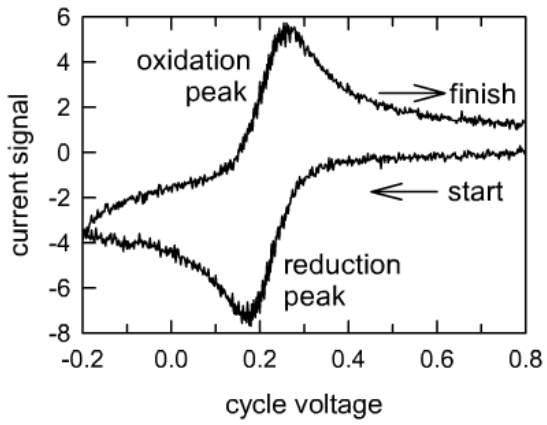

Figure 2.16 A typical cyclic voltammogram [20]

2.7 Corrosion [22]

Corrosion is the deterioration of materials by chemical interaction with their environment. The term corrosion is sometimes also applied to the degradation of plastics, concrete and wood but generally refers to metals. The most widely used metal is iron (usually as steel). There was the accepted theory and it is actually quite simple. The basic requirements for electrochemical corrosion are that anodes and cathodes must be present to form a cell, and direct current must flow. The anodes and cathodes could be close together (local cells) or they could be far apart. The current can be self-induced or impressed on the system from an outside source.

2.7.1 Corrosion Prevention [21]

In virtually all situations, metal corrosion can be managed, slowed or even stopped by using the proper techniques. Corrosion prevention can take a number of forms depending on the circumstances of the metal being corroded.
Corrosion prevention techniques can be generally classified into 6 groups:

- Environmental Modifications
- Metal Selection and Surface Conditions
- Cathodic Protection
- Corrosion Inhibitors
- Coating
- Plating

2.7.2 Chemistry of Corrosion [21]

Virtually all corrosion reactions are electrochemical in nature, at anodic sites on the surface, the iron goes into solution as ferrous ions, this constituting the anodic reaction. As iron atoms undergo oxidation to ions, they release electrons where negative charge would quickly build up in the metal and prevent further anodic reaction, or corrosion. Thus, this dissolution will only continue if the electrons released can pass to a site on the metal surface where a cathodic reaction is possible. At a cathodic site the electrons react with some reducible components of the electrolyte and removed from the metal. The rates of the anodic and cathodic reactions must be equivalent according to Faraday's Laws, being determined by the total flow of electrons from anodes to cathodes which is called the "corrosion current", I_{cor}. Since the corrosion current must also flow through the electrolyte by ionic conduction the conductivity of the electrolyte will influence the way in which corrosion cells operate. The corroding piece of metal is described as a "mixed electrode" since simultaneous anodic and cathodic reactions are proceeding on its surface. The mixed electrode is a complete electrochemical cell on one metal surface.

The Tafel extrapolation method is illustrated in Figure 2.17. The solid curve represents the experimental polarization curve that would be observed, whereas the dashed lines are the extrapolations of the linear branches. The intersection of these extrapolated lines provides the corrosion potential (E_{corr}) and the corrosion current I_{corr}). The Figure 2.17 also illustrates the behavior when concentration polarization is presented and the current is limited, partially or entirely, by the mass transfer of the oxidant to the metal surface.

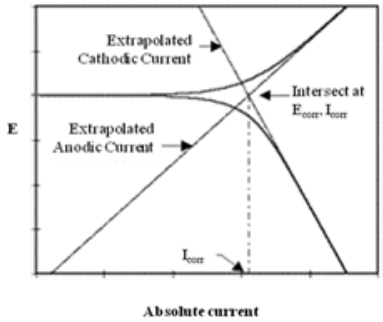

Figure 2.17 Polarization diagram from Tafel extrapolation method [21]

Croatia the most common and important electrochemical reactions in the corrosion of iron are showed as follow:

Anodic reaction (corrosion):

$$Fe \rightarrow Fe^{2+} + 2e^{-} \qquad (2.3)$$

Cathodic reactions (simplified):

$$2H^{+} + 2e^{-} \rightarrow H_2 \qquad (2.4a)$$

or $$H_2O + 1/2O_2 + 2e^{-} \rightarrow 2OH^{-} \qquad (2.4b)$$

$$Fe^{2+} + 2OH^{-} \rightarrow Fe(OH)_2 \text{ , iron (II) hydroxide} \qquad (2.5)$$

Proton reduction (Eq. 2.4a) is most common reaction in acidic medium (pH range 6.5 – 8.5). The most important reaction is oxygen reduction 2.4b. In this latter case corrosion is usually accompanied by the formation of solid corrosion debris from the reaction between the anodic and cathodic products.

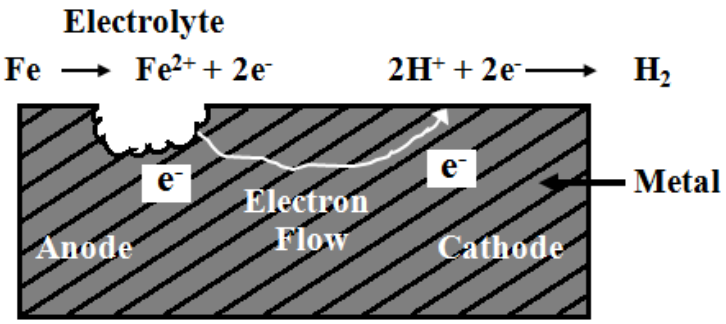

Figure 2.18 Basic diagram showing requirements for corrosion of metals [22]

Pure iron (II) hydroxide is white but the material initially produced by corrosion is normally a greenish color due to partial oxidation in air.

$$2Fe(OH)_2 + H_2O + 1/2O_2 \rightarrow 2Fe(OH)_3 \text{ , hydrated iron (III) oxide} \quad (2.6)$$

2.11 Literature Review

Fei *et al.* [12, 15, 23] studied the preparation of polyaniline/phosphorylated poly(vinyl alcohol) nanoparticles and their aqueous redispersion stability. PAn/P-PVA was prepared by *in situ* chemical oxidation polymerization method [15]. The colloidal PAn/P-PVA dispersions were synthesized by the polymerization of aniline in aqueous acidic media (1M HCl) containing P-PVA. The dark-green colloid PAn/P-PVA dispersion was characterized using FT-IR, TGA, TEM and electrical conductivity. The P-PVA/aniline feeding ratio ranged from 50 to 60, the colloidal PAn/P-PVA nanoparticles showed spherical shape with good uniform, significant re-dispersed stability in aqueous media, and the PAn/P-PVA nanoparticles were possessed of conductivity up to 7 S/cm. The high electrically conductive polyaniline/partially phosphorylated poly(vinyl alcohol) composite films *via* aqueous dispersions was investigated [23]. The effect of feeding ratio of P-PVA/PAn (16.96 to 23.46) onto nanoparticles morphology was also studied. PAn/P-PVA nanoparticles showed spherical shape and the PAn/P-PVA composite films exhibited high degree of crystalline orientation, excellent electrical conductivity, water-resistance property, and mechanical properties. The synthesized technique was further developed based on

green chemical process concern. The conducting polyaniline nanoparticles encapsulated with polyacrylate via emulsifier-free seeded emulsion polymerization and their electroactive films was investigated [12]. Acrylate monomer was selected due to its excellent film-forming performance and mechanical property. The PAn/P-PVA and (PAn/P-PVA)/PAc nonacomposites were characterized by FT-IR, TGA, TEM, SEM, XRD and conductivity. The results of TEM, SEM and XPS indicated the encapsulation of PAc onto PAn/P-PVA nanoparticles. The maximum electroconductivity was achieved at 0.41 S/cm for pellet and 0.05 S/cm for film of PAn/P-PVA/PAc which prepared by 2.402 g PAn/P-PVA nanoparticles (50.93 PAn/P-PVA ratio) and 6 g acrylate monomer.

Suzaki *et al*. [24] studied the ionic conduction in partially phosphorylated poly(vinyl alcohol) as polymer electrolytes. The preparation of P-PVA with dipotassium salts and the effects of phosphorylation on the ionic conduction in the mixed film of P-PVA, polyethylene glycol (PEG) and P-PVA/PEG film were investigated. The P-PVA composites were analyzed by DSC, XRD and temperature dependence of ionic conductivity (DP). The results indicated that the PVA decreased the glass transition temperature ($Tg_)$ values and the activation energy of ionic conduction, and increased the ionic conductivity, which depend on DP. The XRD pattern showed that the amorphous area was extended.

Ying *et al.* [25] studied the preparation and properties of highly phosphorylated poly(vinyl alcohol) hydrogels chemically crosslinked by glutaraldehyde. This work reported the new anionic polyelectrolyte gels by the crosslinking reaction of P-PVA. The products were analyzed by FT-IR, NMR, TGA and DSC. The FTIR results of P-PVA showed the peaks at 1000 cm^{-1} which attributed to the characteristic absorption of C-O-C group in the crosslink P-PVA. The water absorbability depended directly on the crosslinking density and degree of crystallinity in the hydrogel.

Myoung *et al.* [26] studied the polyurethane/polyaniline and polyurethane-poly(methyl methacrylate)/polyaniline conductive core-shell particles: preparation, morphology, and conductivity. The poly(octadecyl acrylate) (PODA) was blended with PAn/dodecyl benzenesulfonic acid (DBSA) complex to form long alkyl chain flexible polymer on the electroactive rigid rod-like $PAn(DBSA)_4$ complex. For the $PAn\ (DBSA)_4$/PODA samples at different composition ratios, a homogenous smectic

liquid-crystalline structures were observed for a PODA content below 10 wt%. This electrochromatic behavior was evidenced by the increased of localized polaron band in UV-vis-NIR absorption spectra and the blue shift anion absorption band related to the electrical conductivity of polyaniline backbone in FT-IR spectra. The homogenous smectic-like liquid-crystalline structure was confirmed by the optical microscopy and XRD when the PODA content is below 20 wt% in the binary blends.

Rout *et al.* [27] studied the development of conducting polyaniline coating: a novel approach to superior corrosion resistance. The synthesis of PAn powder was synthesized through chemical polymerization process. The polymerization was cooled at 0^{o}C by addition HCl acid media of ammonium persulfate (APS). The products obtained were analyzed by FT-IR, DTA/TGA, SEM, conductivity and corrosion testing. The coating was formulated by dispersion PAn powder in a medium oil alkyd. The yield of synthesized powder was found to be 90% with particle sized ranging between 10 and 28 μm. The conductivity of coating increased with an increasing in solid concentration in the range of 10-15 wt%. The corrosion rate of PAn coated on steel in 3.5% NaCl solution was found to be 0.132 millimeter per year (mpy) compared to 3.627 mpy in case of bare steel. The result indicated superior corrosion resistance of PAn coated product.

Il Sang *et al.* [28] studied the preparation of polyaniline coated poly(methyl methacrylate) (PMMA) microsphere by graft polymerization and its electrorheology. The PMMA particles were prepared by dispersion polymerization with uniform size distribution, and they were swollen by glycidyl methacrylate (PGMA) with a radical initiator, benzoyl peroxide (BPO). Core-shell structure of PAn-PGMA particles containing 50 wt% of PAn was synthesized with the same ratio of PMMA and PAn, using monodisperse acrylic microspheres (PAn-PGMA) with aniline on the surface. Synthesized particles were analyzed using various methods such as SEM, TGA, ^{13}C FT-NMR and zeta-potential meter. Since the pristine PAn-PGMA particles right after synthesis were unsuitable for the ER test due to its high conductivity, we therefore this work controlled their high conductivity to semi-conductive by dedoping process of the particles.

Elçin *et al.* [29] studied the improving polyaniline processability by grafting acrylic copolymer. The styrenesulfonate (SSA) of polyaniline/acrylic copolymers

were synthesized via free radical polymerization through polymerization in dispersed medium. The (BuA-co-MAA) and PAn-SSA were characterized using SEM, TGA, FT-IR and electrochemical analysis. Through the applied methodology, electrochemically active PAn-acrylic based materials, with little reduction in the electrical conductivity with respect to the PAn–SSA homopolymer were obtained. Finally, it can be mentioned that the grafting of the acrylic copolymers on the PAn–SSA, using the vinyl group of the styrenesulfonate counterion as the link between the polyaniline and the acrylic copolymer, allowed producing materials with electrical properties highly influenced by the film properties of the acrylic graft copolymer.

Bremer *et al.* [30] studied the preparation of core-shell dispersions with a low tg polymer core and a polyaniline shell. The chemical polymerization of aniline in the presence of sterically stabilized low T_g particles (resins) resulted in a stable dispersion of hybrid particles with a core of the resin and a shell of polyaniline. During this time, many oligomers are formed as can be presented in the color of the reaction mixture and determined in several peaks of the HPLC data. The amounts of aniline, benzidine and dimer were kept constant during this time. If polyurethane particles are used as core, there was no evidence for accumulation of reaction products in the particles. The polyurethane-polyaniline dispersion had a good coating properties and can be prepared by benzidine-free condition.

Chien-Yu *et al.* [31] studied the preparation of polyurethane (PU)/polyaniline and polyurethane-poly(methyl methacrylate) (PU/PMMA)/polyaniline conductive core-shell particles: preparation, morphology, and conductivity. The first stage was a production of core PU or PU-PMMA via miniemulsion polymerization using sodium dodecyl sulfate (SDS) as the surfactant. The second stage was the synthesis of the shell of polyaniline over the surface of core PU or PU-PMMA particles. HCl and DBSA were used as the dopant agents. With a higher DBSA concentration, PU core particles were well covered by PAn polymer and rod-like shape of PAn particles was observed. From the TEM observation, a higher DBSA concentration provided rod-shape PAn particles and a better coverage of PAn polymers over the core surfaces. PU/PAn and PU-PMMA/PAn core-shell latex were synthesized successfully with different concentrations of DBSA.

Moon *et al.* [32] studied the polyaniline coated poly(butyl methacrylate) core-shell particles: roll-to-roll printing of templated electrically conductive structures. The conductive colloidal was composed of core-shell particles where poly(butyl methacrylate) was (PBMA) core particles and polyaniline (PAn) was shell surrounded the PBMA spheres. The synthesis method of the PBMA particles was followed a typical emulsion polymerization. TEM micrograph showed the confirmation of the PAn completely covers the entire surface of the cores.

CHAPTER III

EXPERIMENTAL

3.1 Chemicals

1. Poly(vinyl alcohol), 88%, AR grade : Ajax Finechem
2. Urea, 99%, AR grade : Ajax Finechem
3. Phosphoric acid, 85%, AR grade : Ajax Finechem
4. Aniline, AR grade : Loba Chemie
5. Acrylic acid (AA), 99%, AR grade : Aldrich
6. Methyl methacrylate (MMA), 99%, AR grade : Aldrich
7. Butyl acrylate (BA), 99%, AR grade : Aldrich
8. Ethylene glycol dimethacrylate (EGDMA), 99%, AR grade : Aldrich
9. Ammonium persulfate, AR grade : Ajax Finechem
10. Dimethyl sulfoxide, AR grade : Sigma-Aldrich
11. Ethanol, AR grade : QRëc
12. Methanol, AR grade : QRëc
13. Ammonia solution, 25%, AR grade : QRëc
14. Sodium hydroxide, AR grade : QRëc
15. Hydrochloric acid, 37%, AR grade : QRëc
16. Sulfuric acid, 98%, AR grade : QRëc
17. Nitrogen gas, 99.9% : PraxAir
18. De-ionized water

3.2 Equipment

1. Fourier Transform Infrared Spectrophotometer (FT-IR) : Spectrum GX Perkin Elmer
2. Dynamic Light Scattering : Nanotrac NPA252
3. X-ray Diffractometer (XRD) : Bruker AXS Model D8
4. Thermal Gravimetric Analyzer (TGA) : Perkin-Elmer Pyris Diamond
5. Scanning Electron Microscope (SEM) : JEOL JSM-6400
6. Transmission Electron Microscope (TEM) : JEOL JSM-2100

7. Potentiostat/Galvanostat Instrument : Autolab Type III, model PG stato 30

3.3 Synthesis of Phosphorylated Poly(vinyl alcohol) (P-PVA)

Partially phosphorylate poly (vinyl alcohol) (P-PVA) was prepared by the phosphorylation of PVA with phosphoric acid in an aqueous media as shown in Figure 3.1 and 3.2. Firstly, 0.4 g of urea was added to 33.33 mL of dimethyl sulfoxide (DMSO) in a round bottom flask equipped with condenser and nitrogen gas inlet. The mixture was stirred for 1 h. and heated up to 120 ^{o}C. Then 6.67 mL orthophosphoric acid in 100 mL of DMSO was added. The mixture was heated up to 130 ^{o}C and 4.0 g of PVA was then added and stirred thoroughly for 80 min under nitrogen atmosphere. The yellowish solution was obtained. The resulting solution was precipitated by methanol to obtain the white precipitate P-PVA. Finally, the white precipitate was dried in vacuum oven at 50 ^{o}C.

3.4 Synthesis of Polyaniline/Partially Phosphorylated Poly (vinyl alcohol) (PAn/P-PVA) Nanoparticles by *In Situ* Chemical Oxidation Polymerization

The PAn/P-PVA nanoparticles was synthesized by *in situ* chemical oxidation polymerization as shown in Figure 3.3. Aniline monomer polymerization was performed in 0.5M HCl aqueous media with by using ammonium persulfate ($(NH_4)_2.S_2O_8$) as an oxidant/initiator and P-PVA as a stabilizer and co-dopant. 4.0 g aniline was well mixed with 240 mL of 0.5 M HCl aqueous solution containing 2.4 g P-PVA. The reaction mixture was vigorously stirred at 0°C (Figure 3.5(a)) followed by the addition of 60 mL 0.5M HCl aqueous solution of ammonium persulfate. The polymerization was allowed to proceed for 6 h while maintaining the temperature of 0 ± 2 ◦C. Dark green PAn/P-PVA colloidal was obtained. The dispersion of PAn/P-PVA was obtained by precipitation, filtration and followed by washing with 80/20 distilled water/ethanol (v/v) mixture and drying in vacuum oven at 60°C for 48 h. The structure of PAn/P-PVA nanocomposite is shown in Figure 3.4(a).

3.5 Encapsulation of PAn/P-PVA Nanoparticles with Polyacrylate

The scheme of (PAn/P-PVA)/PAc preparation is shown in Figure 3.3. Acrylate monomers (made up by 2 wt.% of acrylic acid (AA), 44 wt.% of methyl methacrylate (MMA), and 50 wt.% of butyl acrylate (BA)) were used as monomers to encapsulate the PAn/P-PVA nanoparticles. 4% ethylene glycol dimethacrylate (EGDMA) was used as crosslinking agent to restrict the penetration of the acrylate monomers into the PAn/P-PVA particles (Figure 3.4(b)). Specifically in this work, PAn/P-PVA nanoparticles were re-dispersed in the round bottom flask containing 90 mL of 1M ammonia solution and placed in ultrasonic bath for 1 h. Then, acrylate monomers were fed into the flask under starved-feed addition. Simultaneously, ammonium persulfate (APS) aqueous solution (1.25 g of APS was dissolved in distilled water) was fed into the flask with an appropriate dropping rate to initiate the polymerization of acrylate monomers. The reaction temperature was maintained at 75 ^{o}C for 5 h (Figure 3.5(b)). The obtained polyaniline/partially phosphorylated poly (vinyl alcohol)/polyacrylate ((PAn/P-PVA)/PAc) emulsion was cooled down to room temperature. The (PAn/P-PVA)/PAc composite nanoparticles were dried at 40 ◦C under vacuum for 24 h for the further analysis. The effects of total acrylate volume loading were studied over the range of 4.81%, 7.21% and 9.62% v/v based on total volume of 1M ammonia solution as shown in Table 3.1.

The monomer conversion and solid content was determined by gravimetric method as follows:

$$Monomer\,Conversion(\%) = \frac{M_0 - M_1}{M_2} x100 \qquad (3.1)$$

$$Solid\ content\ (\%) = (M_0 / M_3)\ x\ 100 \qquad (3.2)$$

Where M_0 = Mass of the resulting composite particles (gram)

M_1 = Mass of the charged PAn/P-PVA nanoparticles (gram)

M_2 = Mass of the charged acrylate monomer (gram)

M_3 = Mass of (PAn/P-PVA)/PAc solute (gram)

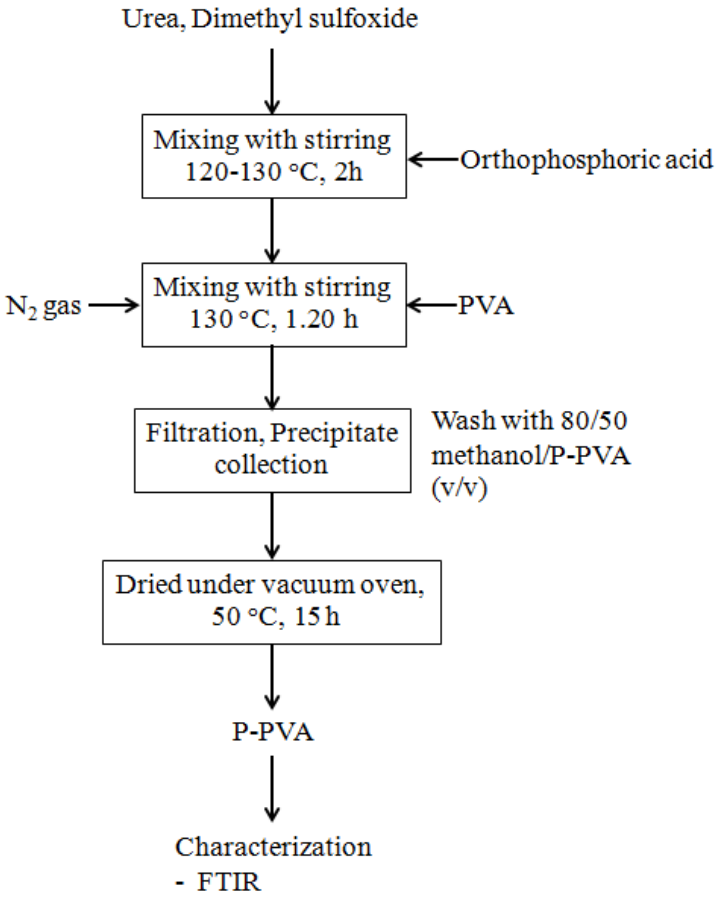

Figure 3.1 Synthesis of phosphorylation of PVA

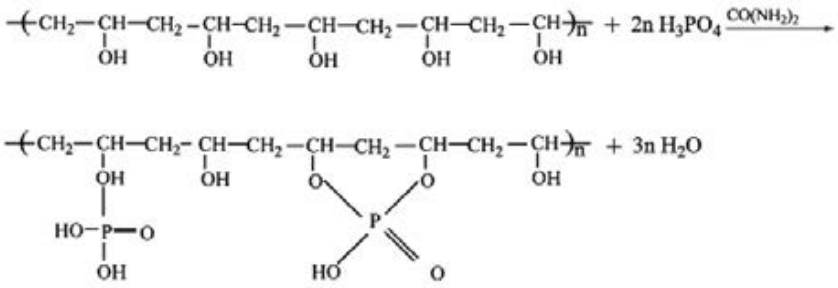

Figure 3.2 Schematic of phosphorylation of PVA

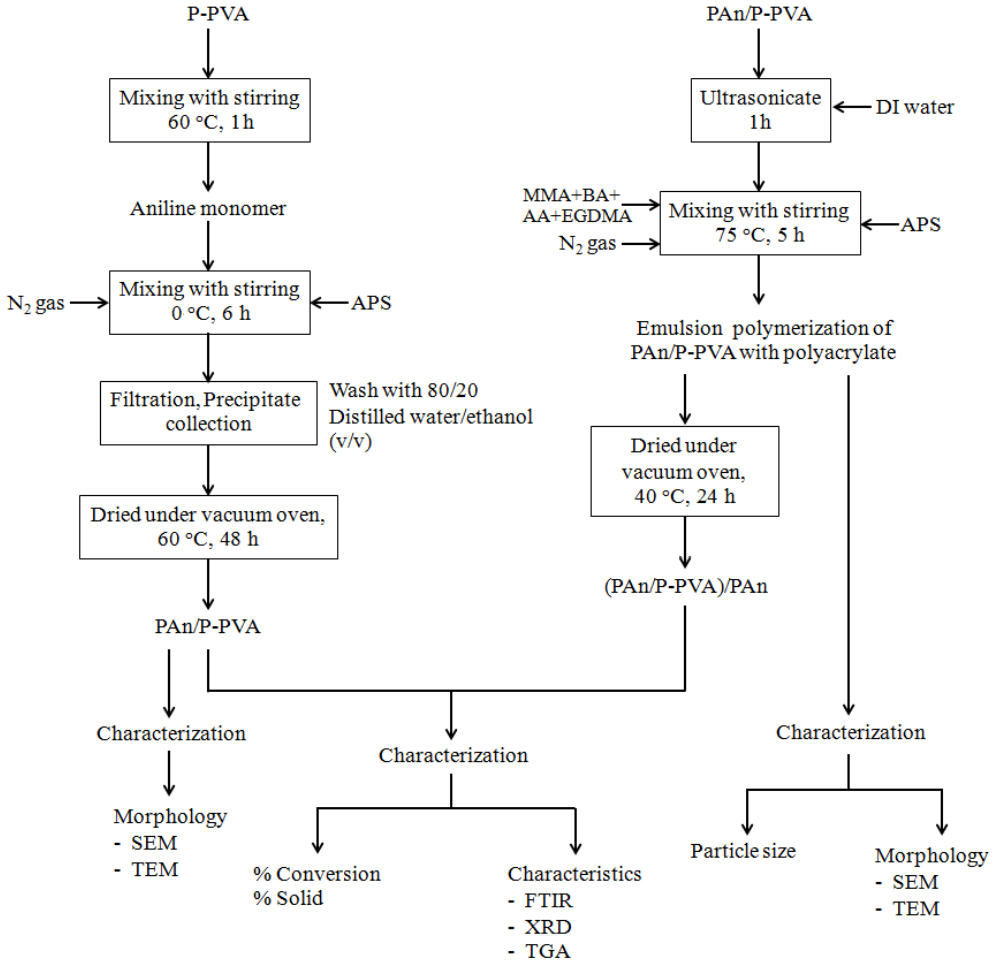

Figure 3.3 Chemical oxidation polymerization of PAn/P-PVA and Emulsion polymerization of (PAn/P-PVA)/PAc nanoparticles

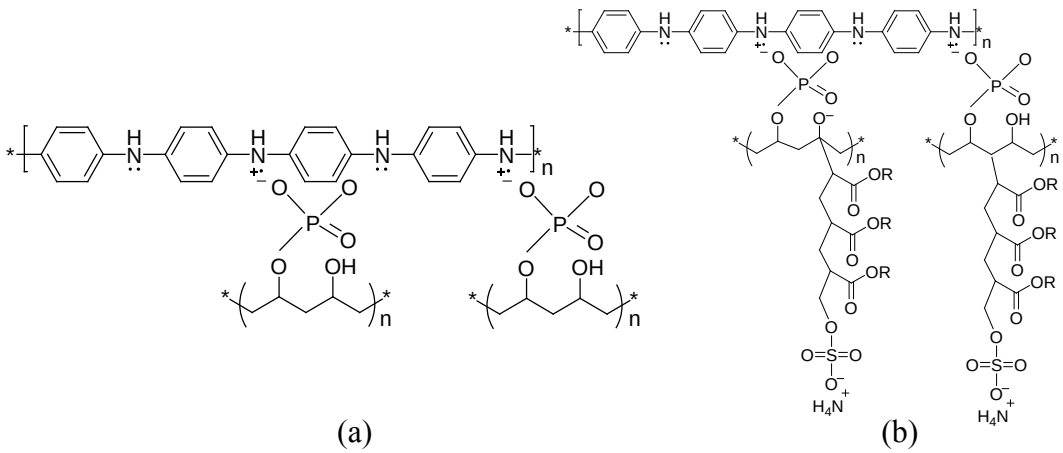

Figure 3.4 Chemical structure of (a) PAn/P-PVA and (b) (PAn/P-PVA)/PAc

Table 3.1 % Total volume of acrylate monomers containing 90 mL of 1M ammonia solution

PAn/P-PVA loading (g)	Acrylate amount (g)	Acrylate volume (cm^3)	Total acrylate* (% v/v)
0.3	4	4.33	4.81
	6	6.49	7.21
	8	8.66	9.61
0.5	4	4.33	4.81
	6	6.49	7.21
	8	8.66	9.61
0.7	4	4.33	4.81
	6	6.49	7.21
	8	8.66	9.61

* Total acrylate (% v/v) was calculated from percentage of acrylate volume per 1M ammonia volume

(a) (b)

Figure 3.5 (a) Chemical oxidation polymerization of PAn/P-PVA nanoparticles
(b) Emulsion polymerization of (PAn/P-PVA)/PAc nanoparticles

3.6 Characterization

3.6.1 Fourier Transform Infrared (FT-IR) Spectroscopy

Structures of PAn/P-PVA and (PAn/P-PVA)/PAc nanoparticles were characterized using a Spectrum GX Perkin Elmer in the range of 400-4000 cm^{-1}. The samples were prepared by dispersion in potassium bromide (KBr) and pressing into pellets.

3.6.2 Particle Size Measurement

The number-average particle diameter ($\overline{D}_n$) and particle size distribution (PSD) of (PAn/P-PVA)/PAc nanoparticles were examined using Dynamic light scattering (DLS, the Nanotrac NPA252). PAn/P-PVA or (PAn/P-PVA)/PAc nanoparticles samples were dispersed into DI water. The number-average particle diameter ($\overline{D}_n$) and particle size distribution were measured three times. The average values with standard deviation were reported.

3.6.3 Thermogravimetric Analysis (TGA)

Thermogravimetric analysis (TGA) was performed using a Perkin-Elmer Pyris Diamond TG/DTA. 10-13 mg of samples was heated from 40°C to 800°C with heating rate of 10°C/min under nitrogen atmosphere. The initial decomposition temperature (T_{id}) and the temperature at the maximum mass loss rate (T_{max}) were recorded.

3.6.4 X-ray Diffraction (XRD)

X-ray diffraction (XRD) measurements were performed using a Bruker AXS Model D8 Discover with CuKα X-ray radiation (1.5406 Å) at 40 kV and 40 mA. The samples were scanned in the 2θ range from 1° to 35°, with a step time of 0.3 s/step and a step size of 0.02°. The measurements were operated by Evaluation (EVA) program.

3.6.5 Morphological Study

The morphology of PAn/P-PVA and (PAn/P-PVA)/PAc nanoparticles was investigated by scanning electron microscope (SEM, JEOL Model JSM-5410 LV). The completely dried samples were placed on a SEM stub and arranged in a single layer without clustered and then coated with gold.

The sample was dried so that moisture in the sample could not interfere with polymerization of acrylate monomers and affect adhesion. The nanoparticles morphology was characterized by using transmission electron microscope (TEM, a JEOL JEM-2100) at accleration voltage of 80 kV. The dilute nanoparticles was deposited on Cu grid and stained with 1% (v/v) of osmium tetroxide (OsO_4) for 24 h.

3.6.6 Cyclic Voltammetry

The electrochemical behavior of the (PAn/P-PVA)/PAc coated on carbon fiber cloth used as working electrode (Figure 3.4a) in 0.5 M HCl aqueous solution were investigated by cyclic voltammogram (CV) as shown in Figure 3.4b. The electrochemical behavior was studied at the potential range of -1.25V to +1.25V and scan rate of 50 mV/S. A Pt counter electrode and an Ag/AgCl reference electrode were used throughout of the studies.

Program : GPES

Method : cyclic voltammetry : normal

Parameter of potentials

Number of scans	:	5
Start potential (V)	:	1.0
First vertex potential (V)	:	-1.25
Second vertex potential (V)	:	+1.25
Step potential (V)	:	0.0195
Scan rate (V/s)	:	0.05
Surface area (cm^2)	:	2.3

(a)

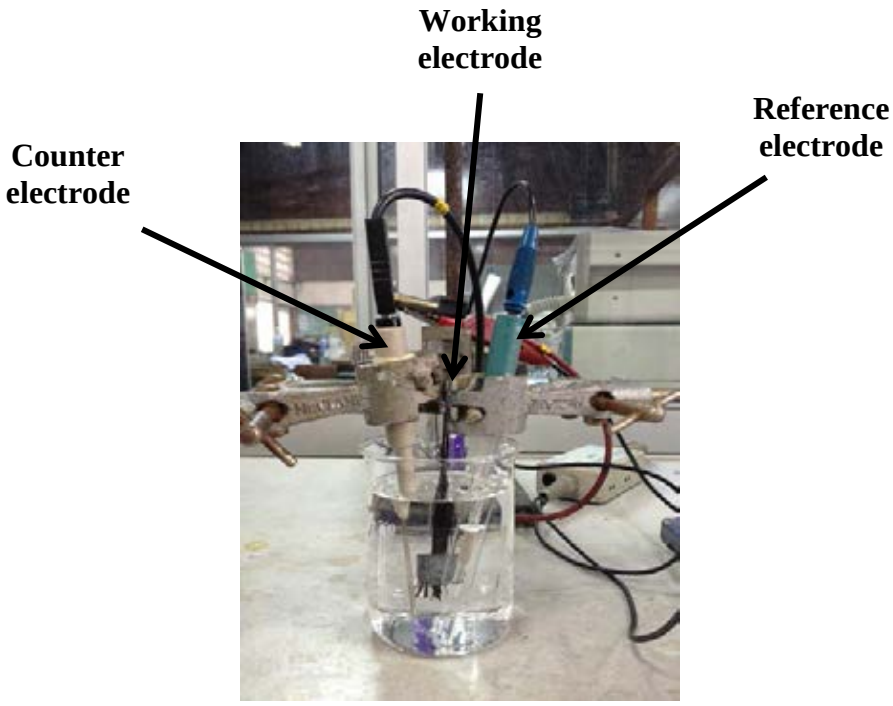

(b)

Figure 3.6 (a) Coated PAn/P-PVA and (PAn/P-PVA)/PAc nanocomposites on carbon fiber cloth as working an electrode (b) Cyclic voltammogram of PAn/P-PVA and (PAn/P-PVA)/PAc nanocomposites

3.6.7 Corrosion Study

The electrochemical Tafel slope analysis was used to evaluate the anticorrosive performance of (PAn/P-PVA)/PAc nanocomposites coating on steel samples as shown in Figure 3.5. Tafel plots for (PAn/P-PVA)/PAc coated steel samples were recorded by sweeping the potential from equilibrium potential toward negative and positive potentials against Ag/AgCl reference electrode in 1M H_2SO_4 electrolyte.

Program : GPES

Method : linear sweep voltammetry (staircase) : normal

Parameter of corrosion rate

Edit procedure – Page1

- Begin potential (V)	:	- 0.3
- End potential (V)	:	+ 0.3
- Step potential (V)	:	0.001
- Scan rate (V/s)	:	0.001
- Surface area (cm^2)	:	2.3

Edit procedure – Page 2

- Define (vertex) potential OCP	=	active
- Time to with for OCP (s)	:	0
- Tafel plot	=	active

(a)

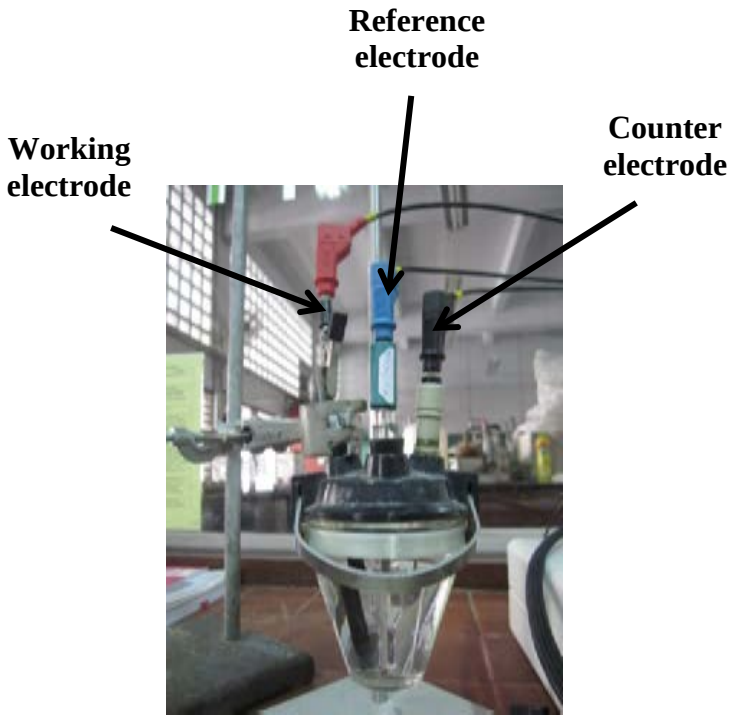

(b)

Figure 3.7 Anticorrosion performance testing (a) Electrochemical Tafel slope analysis of (PAn/P-PVA)/PAc nanocomposites coating on steel samples (b) electrode configuration

CHAPTER IV

RESULTS AND DISCUSSION

Polyaniline/partially phosphorylated poly(vinyl alcohol)/polyacrylate (PAn/P-PVA)/PAc nanoparticles were successfully prepared by the encapsulation of the polyaniline/partially phosphorylated poly (vinyl alcohol) (PAn/P-PVA) nanoparticles with polyacrylate (PAc) via emulsifier-free seeded emulsion polymerization using ammonium persulfate as an oxidant/initiator. The reaction mixture was vigorously stirred at 75°C for 5 h. The particle size of (PAn/P-PVA)/PAc nanoparticles in water was investigated by dynamic light scattering method. The monomer conversion and solid content of (PAn/P-PVA)/PAc nanoparticles were determined. The PAn/P-PVA and (PAn/P-PVA)/PAc nanoparticles were also characterized by Fourier-transform infrared spectroscopy (FT-IR) and X-ray diffraction (XRD). The surface morphology of nanoparticles were observed by scanning electron microscopy (SEM) and transmission electron microscopy (TEM). Thermal properties of the PAn/P-PVA and (PAn/P-PVA)/PAc nanoparticles were examined by thermogravimetric analysis (TGA). The electrochemical behavior of the (PAn/P-PVA)/PAc nanocomposites was investigated by cyclic voltammetry (CV). The electrochemical Tafel slope analysis was used to evaluate the anticorrosive performance of (PAn/P-PVA)/PAc nanocomposites coating on steel samples.

4.1 Synthesis of PAn/P-PVA Nanoparticles Encapsulated with Polyacrylate via Emulsifier-free Seeded Emulsion Polymerization

The encapsulation of the PAn/P-PVA nanoparticles with polyacrylate (PAc) was accomplished by the emulsifier-free seeded emulsion polymerization (Figure 4.1). In this work, the P-PVA was used as a surfactant and co-dopant for the formation of PAc covered the PAn/P-PVA nanoparticles to obtain (PAn/P-PVA)/PAc

nanoparticles. The effect of PAc concentration on monomer conversion, solid content, average particle size ($\overline{D}_n$) and particle size distribution (PSD) of (PAn/P-PVA)/PAc nanoparticles are shown in Table 4.2 and Figure 4.2

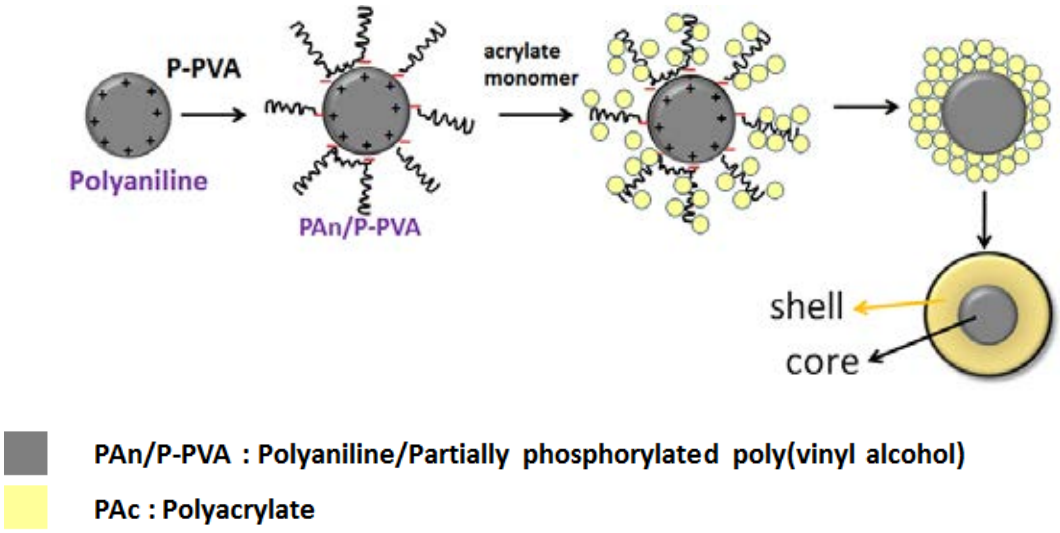

Figure 4.1 Schematic of encapsulate PAn/P-PVA nanoparticles with PAc

The monomer conversion decreased and solid content increased with an increasing acrylate amount (4-8 g) at the constant amount of PAn/P-PVA (0.3-0.7 g). For (PAn/P-PVA)/PAc-4b, the monomer conversion was maximum at 93.9% whereas for (PAn/P-PVA)/PAc-6b and (PAn/P-PVA)/PAc-8b loading the monomer conversion was 77.7% and 70.1%, respectively. It is possible that an increasing acrylate amount caused the micelle nucleation around the surface of PAn/P-PVA. Micelle capacity limitation was due to the low amount of surfactant and the excess monomer could not transfer into micelles. Therefore, excess amount of the acrylate monomer caused low stability of emulsion polymerization resulting in low monomer conversion in the system due to the acrylate monomer did not covering PAn/P-PVA nanoparticles. The similar results were earlier reported for synthesis of (PAn/P-PVA)/PAc via emulsifier-free seeded emulsion polymerization [15, 30]. For high loading of PAn/P-PVA (0.7 g), the solid content of (PAn/P-PVA)/PAc emulsion was 4.7, 6.0 and 6.8%, respectively for 4, 6 and 8 g of acrylate amount. The results indicated that at high acrylate amount, PAc encapsulated PAn/P-PVA nanoparticles and more aggregation of (PAn/P-PVA)/PAc particles occurred resulting in increasing solid content.

The averge particle size ($\overline{D}_n$) and particle size distribution (PSD) of PAn/P-PVA and (PAn/P-PVA)/PAc nanoparticles at various acrylate amounts are shown in Tables 4.1, 4.2, Figure 4.3. It can be seen that the $\overline{D}_n$ and PSD of PAn/P-PVA were 74.6 and 16.5 nm and % conversion was 49.7%. The effect of acrylate amount was studied over the range of 4-8 g. The averge particle size ($\overline{D}_n$) of PAn/P-PVA-a, PAn/P-PVA-b and PAn/P-PVA-c were increased from 178.1 to 193.3 nm, 145.7 to 186 nm and 147.6 to 239.9 nm respectively with increasing acrylate amount (4-8 g). The averge particle size ($\overline{D}_n$) increased with increasing acrylate amount due to the encapsulation of PAn/P-PVA as a core with polyacrylate (PAc) as a shell. The particle size distribution (PSD) of (PAn/P-PVA)/PAc nanoparticles indicated the unimodal particle size distribution with the presence of the highly aggregated (PAn/P-PVA)/PAc particles. Therefore, the large particle size of (PAn/P-PVA)/PAc was produced due to the aggregation of PAn/P-PVA. For (PAn/P-PVA)/PAc nanoparticles, at the optimal acrylate amount gave high stability of emulsion with (PAn/P-PVA)/PAc-4b due to some shacking time then nanoparticle was slowly precipitate in aqueous media as shown in Figure 4.2. Thus, for the 0.5 g PAn/P-PVA loading, high monomer conversion of 93.9% and 77.7%, small particle size of around 145.7 and 182 nm and high solid content of 4.9% and 5.6% were obtained at an appropriate acrylate amount of 4 and 6 g, respectively.

Table 4.1 Monomer conversion, solid content, average particle size ($\overline{D}_n$) and particles size distribution (PSD) of PAn/P-PVA nanoparticles

Experimental	**PAn/P-PVA**
% Conversion	49.7
% Solid Content	0.62
$\overline{D}_n$ (nm)	74.6
PSD (nm)	16.5

Table 4.2 Effect of acrylate amount on monomer conversion, solid content, average particle size ($\overline{D}_n$) and particles size distribution (PSD) of PAn/P-PVA nanoparticles

Experiment	Total acrylate (% v/v)	% Conversion	% Solid Content	$\overline{D}_n$ (nm)	PSD (nm)
0.3 g (PAn/P-PVA) loading					
(PAn/P-PVA)/PAc-4a	4.81	76.6	3.9	178.1	76.0
(PAn/P-PVA)/PAc-6a	7.21	63.1	4.7	187.0	96.1
(PAn/P-PVA)/PAc-8a	9.61	49.9	4.8	193.3	66.5
0.5 g (PAn/P-PVA) loading					
(PAn/P-PVA)/PAc-4b	4.81	93.9	4.9	145.7	57.9
(PAn/P-PVA)/PAc-6b	7.21	77.7	5.6	182.0	92.8
(PAn/P-PVA)/PAc-8b	9.61	70.1	6.5	186.0	105.0
0.7 g (PAn/P-PVA) loading					
(PAn/P-PVA)/PAc-4c	4.81	85.6	4.7	147.6	83.9
(PAn/P-PVA)/PAc-6c	7.21	74.4	6.0	179.1	89.6
(PAn/P-PVA)/PAc-8c	9.61	65.4	6.8	239.9	95.4

* Total acrylate (% v/v) was calculated from percentage of acrylate volume per 1M ammonia volume

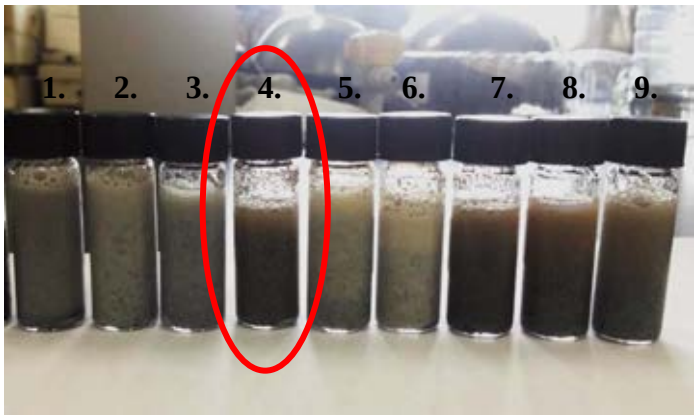

Figure 4.2 Appearance of (PAn/P-PVA)/PAc for 0.3 (1-3), 0.5 (4-6) and 0.7 (7-9) (PAn/P-PVA) loading and 4, 6 and 8 g acrylate amount

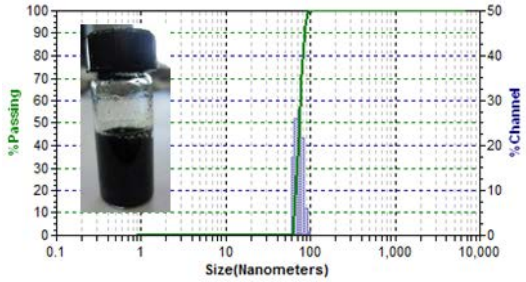

(a) PAn/P-PVA

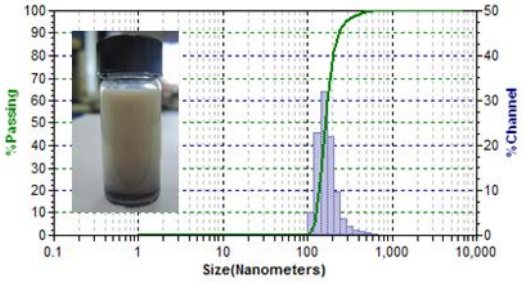

(b) (PAn/P-PVA)/PAc-4a

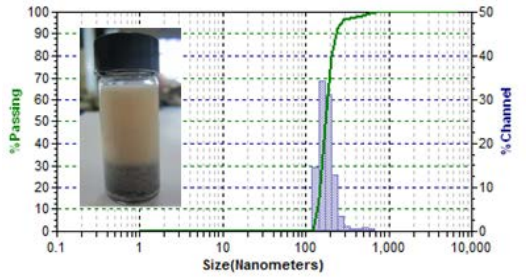

(c) (PAn/P-PVA)/PAc-6a

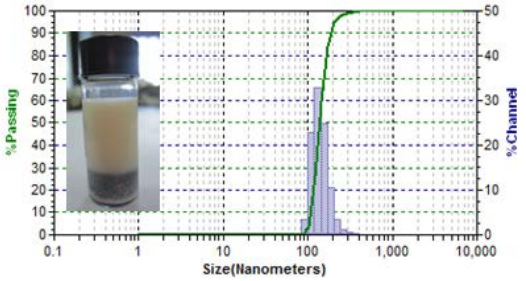

(d) (PAn/P-PVA)/PAc-8a

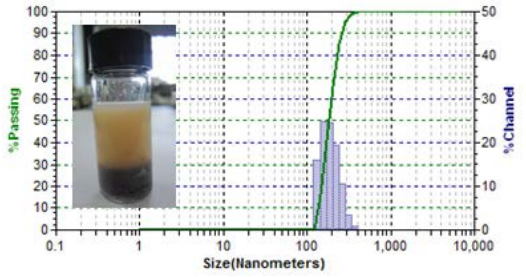

(e) (PAn/P-PVA)/PAc-4b

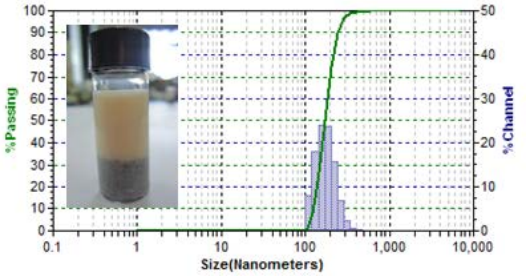

(f) (PAn/P-PVA)/PAc-6b

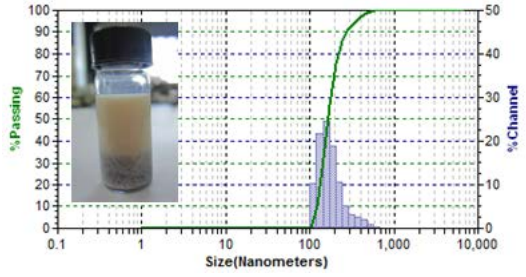

(g) (PAn/P-PVA)/PAc-8b

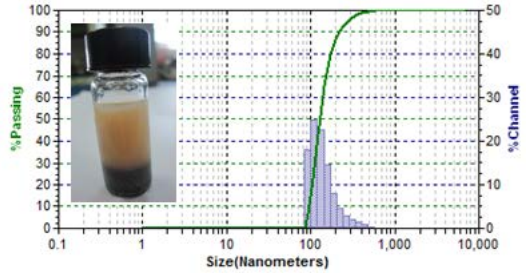

(h) (PAn/P-PVA)/PAc-4c

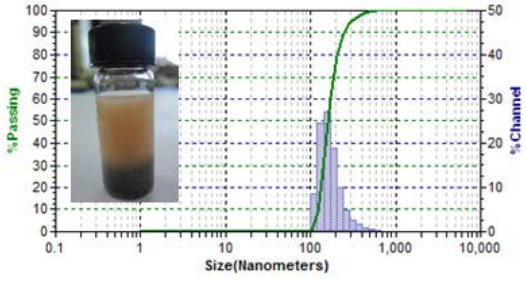

(i) (PAn/P-PVA)/PAc-6c

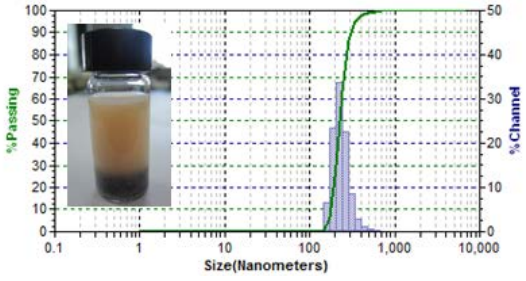

(j) (PAn/P-PVA)/PAc-8c

Figure 4.3 Histograms of particle size distribution of (PAn/P-PVA)/PAc for 0.3, 0.5

and 0.7 PAn/P-PVA loading and 4, 6 and 8 g acrylate amount

4.2 Characterization of PAn/P-PVA and (PAn/P-PVA)/PAc Nanoparticles

4.2.1 FT-IR Analysis

The structure of PAn/P-PVA (a) and (PAn/P-PVA)/PAc (b) nanoparticles are shown in Figure 3.4. FTIR spectra of PAn, P-PVA, PAn/P-PVA, PAc and (PAn/P-PVA)/PAc nanoparticles are shown in Figures 4.4 and 4.5. For the FTIR spectrum of PAn (Figure 4.4(a)), the peaks at 3435, 1566 and 1484 cm^{-1} are assigned to the N-H stretching, the C=N stretching of quinoid ring [12, 23] and the C=C stretching of benzenoid ring, respectively. The peak at 1293 cm^{-1} is attributed to the stretching vibration of the C-N (mode of -N-benzenoid-N-). Peaks at 1109 and 794 cm^{-1} correspond to the in-plane-bending vibration of the C-H (mode of -N=quinoid=N- and quinoid=N^{+}H-benzenoid) and the C-H out-of-plane bending of 1, 2-ring, respectively. In the spectrum of the P-PVA (Figure 4.4(b)), the peaks at 3282, 2910, 1660, 1014 and 950 cm^{-1} are assigned to the O-H stretching, the stretching vibration of the C-H(CH_2), the stretching vibration of the -P=O- groups, the stretching frequency of the -P-O-C- groups and the P-O stretching, respectively. In the spectrum of the PAn/P-PVA nanoparticles (Figure 4.4(c)), the strong absorbance peak at 1127 cm^{-1} is attributed to the overlap of the absorbance frequency of the -P-O-C- groups of P-PVA, the in-plane-bending vibration of the C-H of PAn and the N-Q-N (Q denotes quinoid ring) stretching mode. The peaks at 2917, 1565, 1483, 1296, 1243 and 797 cm^{-1} are assigned to the stretching vibration of the C-H(CH_2), the stretching vibration of the -P=O- groups of P-PVA, the stretching vibration of benzenoid rings of PAn, the stretching vibration of the C-H with aromatic conjugation, the stretching of the C-N of benzenoid ring and the C-H out-of-plane bending of 1, 2-ring, respectively. The obvious increasing the absorbance intensity at 3435 cm^{-1} of the PAn/P-PVA sample is related to the O-H stretching, compared with that of the PAn. The result suggests that the P-PVA molecules had been adsorbed in the PAn nanoparticles.

FTIR spectrum of PAc (Figure 4.5(a)) presents the characteristic bands of the N-H stretching at 3440 cm^{-1}, the O-H stretching around 3218 cm^{-1}, the C-H stretching at 2958 and 2875 cm^{-1}, the C=O stretching at 1732 cm^{-1}, the N-H bending at 1568

cm^{-1}, the bending of CH_2 groups at 1447 cm^{-1}, the bending of CH_3 groups at 1435 and 1403 cm^{-1}, the N-H bending at 1568 cm^{-1}, the S=O stretching at 1238 and 1163 cm^{-1}, the C-O stretching at 1146 cm^{-1} and the S-O stretching at 991, 843 and 756 cm^{-1}, respectively. FTIR spectrum of the (PAn/P-PVA)/PAc nanoparticles (Figure 4.5(b)), shows the decreasing characteristic bands of O-H stretching at 3205 cm^{-1}, the stretching vibration of the C-H(CH_2) at 2955 cm^{-1} and C=O at 1725 cm^{-1} group of the PAc, the stretching vibration of the -P=O- groups of the P-PVA at 1585 cm^{-1}, the stretching vibration of benzenoid ring at 1494 cm^{-1}, the overlap of the absorbance frequency of the CH_2 groups and CH_3 groups of PAc at 1450 and 1407 cm^{-1} respectively, the C-H stretching with aromatic conjugation at 1303 cm^{-1}, the N-Q-N (Q denotes quinoid ring) stretching mode at 1102 cm^{-1} and the out-plane-bending vibration of the C-H at 831 cm^{-1}. The result suggests the successful incorporation of PAc onto the PAn/P-PVA nanoparticles.

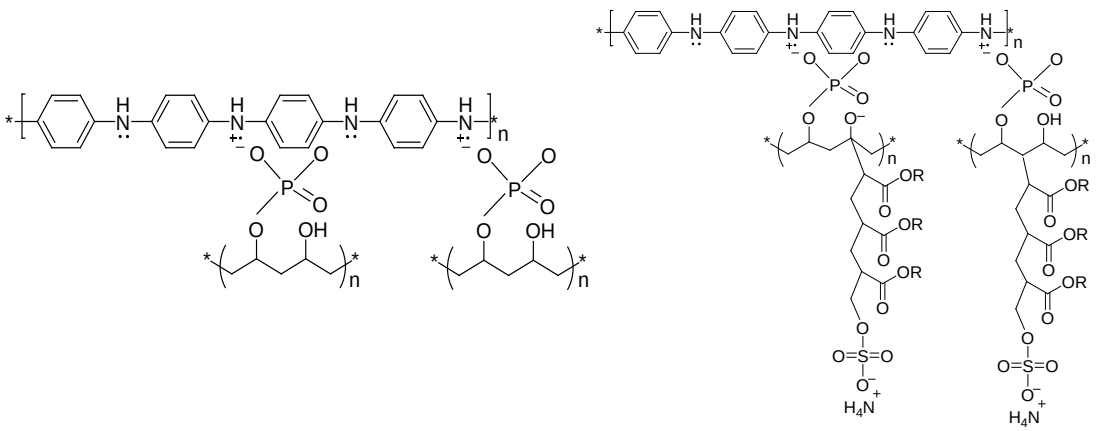

(a) (b)

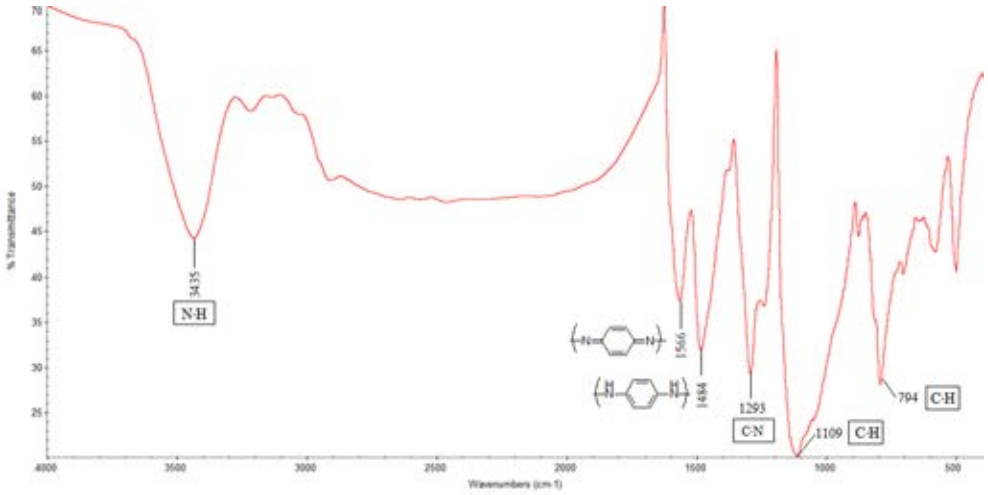

(a) PAn

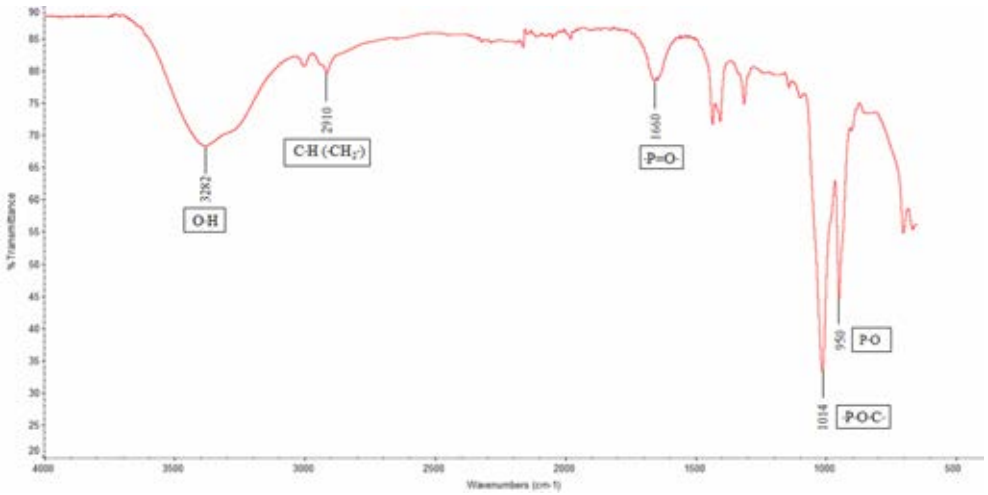

(b) P-PVA

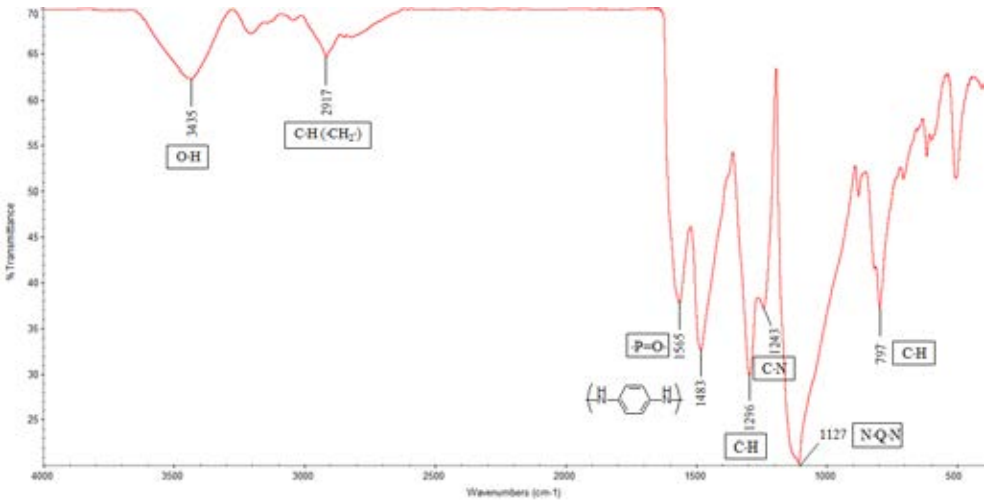

(c) PAn/P-PVA nanoparticles

Figure 4.4 FTIR spectra of (a) PAn, (b) P-PVA and (c) PAn/P-PVA nanoparticles

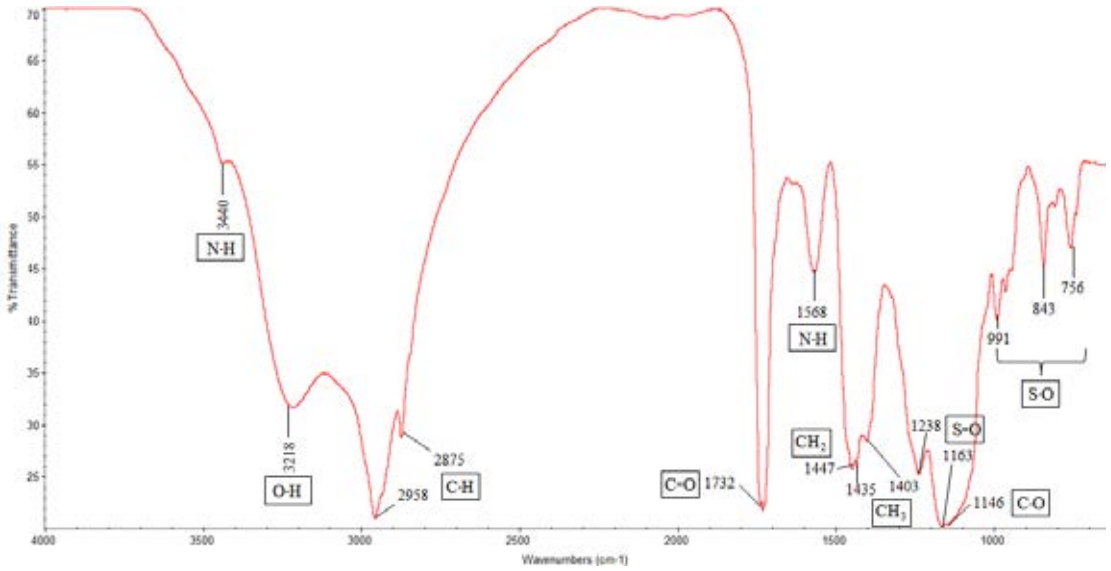

(a) PAc

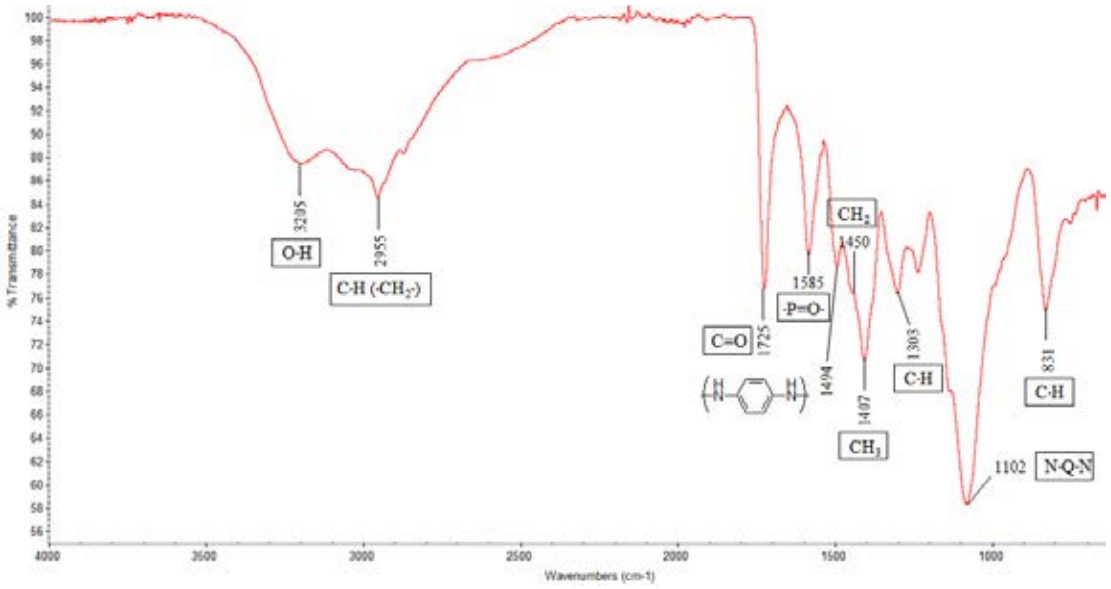

(b) (PAn/P-PVA)/PAc nanoparticles

Figure 4.5 FTIR spectra of (a) PAc and (b) (PAn/P-PVA)/PAc nanoparticles

4.2.2 Thermogravimetric Analysis

Figures 4.6 illustrates the TGA curves and derivative curves (DTG curves) of the PAn/P-PVA, (PAn/P-PVA)/PAc nanoparticles at 0.3, 0.5 and 0.7 g PAn/P-PVA loading and 4, 6 and 8 g of acrylate amount. The acrylate amount affected the decomposition temperature of (PAn/P-PVA)/PAc nanoparticles as summarized in Table 4.3. The thermogram of PAn/P-PVA nanoparticles showed three main degradation steps. The initial decomposition temperature of PAn-P-PVA nanoparticles about 100°C was due to the moisture-losing, the mass loss between 197°C and 308°C was regarded to the decomposition of the H-bonded water of the P-PVA and the de-doping of the doped HCl. The decomposition at temperature range of 363-510°C was due to the breakage of the main chains of both P-PVA and PAn.

Thermal degradation of (PAn/P-PVA)/PAc at various amount of acrylates (4, 6, 8 g) exhibited different thermal behavior with respect to amount of acrylate in the PAn-P-PVA nanoparticles. The results showed the trend of three main degradation steps. The mass loss occurred in the temperature range of 200-320°C due to the loss of the H-boned water and PAc while the shape mass loss after 340 °C is mainly attributed to the breakage of the main chains of the PAn/P-PVA nanoparticles. The residue weight above 500°C is the residual mass of the PAn/P-PVA nanoparticles due to no residual mass of the PAc above 500 °C. The experimental data are good agreement with previous work [29]. Significantly, the residual weight percentages of PAn/P-PVA-c nanoparticles (Table 4.3) at 800 °C were estimated to be 16.8 wt.%, 9.8 wt.% and 7.5 wt.% for the 4, 6 and 8 g of acrylate amount, respectively. The increasing acrylate amount caused decreasing residual weight percentage due to the complete encapsulation of PAn/P-PVA nanoparticles with PAc. For (PAn/P-PVA)/PAc-8c nanoparticles, with the strawberry shape, the residual weight at 800°C was minimum compared to others nanoparticles (see TEM section (PAn/P-PVA)/PAc-4c, (PAn/P-PVA)/PAc-8c). This result implied high thermal stability of (PAn/P-PVA)/PAc nanoparticles. The strawberry shape particles of (PAn/P-PVA)/PAc-8c exhibited greater weight loss than others nanoparticles because the

small molecules in the strawberry structure were easily burned, therefore the result shows the low residual weight.

The results also showed that the (PAn/PVA)/PAc-8c (8 g acrylate amount) had a lowest thermal stability due to a lowest residual weight compared with 4 and 6 g of acrylate amount at the same temperature (800^{o}C). The residual weight in case of (PAn/P-PVA)/PAc-a was 13.0 wt.%, 6.3 wt.% and 8.0 wt.% and (PAn/P-PVA)/PAc-b was 13.2 wt.%, 5.0 wt.% and 8.0 wt.% when heated up at 800 °C for 4, 6 and 8 g of acrylate amount, respectively. These results indicated that increasing acrylate amount decreased the residual weight. However for (PAn/P-PVA)/PAc-a and (PAn/P-PVA)/PAc-b at 6 and 8 g acrylate amount, residual weight increased with increasing acrylate amount. The results are different from thermogram behaviors, which was possibly due to the imperfect encapsulation of the PAn/P-PVA nanoparticles at high acrylate amount. These encapsulation defects imply that PAc matrix was aggregated itself. Therefore, the increasing acrylate amount (6 and 8 g) increased a thermal stability.

Table 4.3 Weight loss (%), initial degradation temperatures (°C) maximum temperature and residual weight of PAn/P-PVA and (PAn/P-PVA)/PAc nanoparticles.

Sample	Loss of water			Loss of organic compounds			Polymer chain breakage			Residual weight (%)
	%wt Loss	T_{id} (°C)	T_{max} (°C)	%wt Loss	T_{id} (°C)	T_{max} (°C)	%wt Loss	T_{id} (°C)	T_{max} (°C)	
PAn/P-PVA	6.0	60	100	7.0	197	308	9.8	363	510	42
0.3 g PAn/P-PVA loading										
(PAn/P-PVA)/PAc-4a	2.5	62	108	14.0	208	310	55.0	348	465	13.0
(PAn/P-PVA)/PAc-6a	2.7	62.5	110	12.5	220	305	66.0	340	478	6.3
(PAn/P-PVA)/PAc-8a	3.0	59	107	12.3	210	303	62.5	342	480	8.0
0.5 g PAn/P-PVA loading										
(PAn/P-PVA)/PAc-4b	1.9	63	115	18.2	228	308	50.0	360	470	13.2
(PAn/P-PVA)/PAc-6b	2.1	65	116	17.0	220	311	58.3	345	488	5.0
(PAn/P-PVA)/PAc-8b	2.7	65	120	15.0	222	308	60.7	341	490	8.0
0.7 g PAn/P-PVA loading										
(PAn/P-PVA)/PAc-4c	1.5	70	122	23.0	198	320	58.0	350	490	16.8
(PAn/P-PVA)/PAc-6c	2.0	72	127	14.0	200	311	59.8	359	492	9.8
(PAn/P-PVA)/PAc-8c	1.4	69	128	14.0	208	308	60.0	361	500	7.5

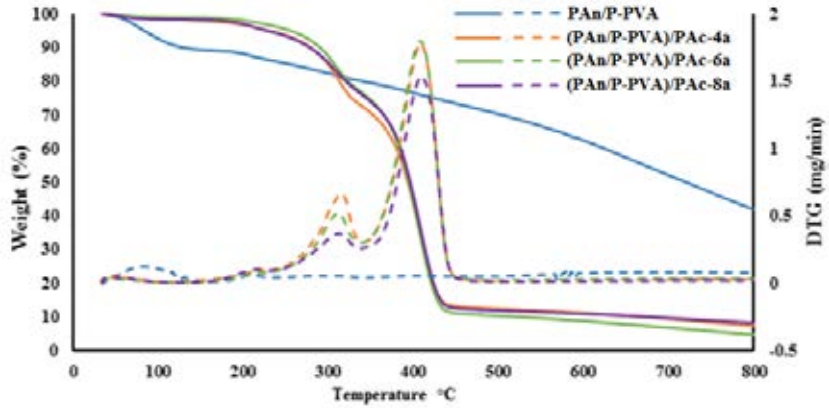

(a) 0.3 g PAn/P-PVA loading

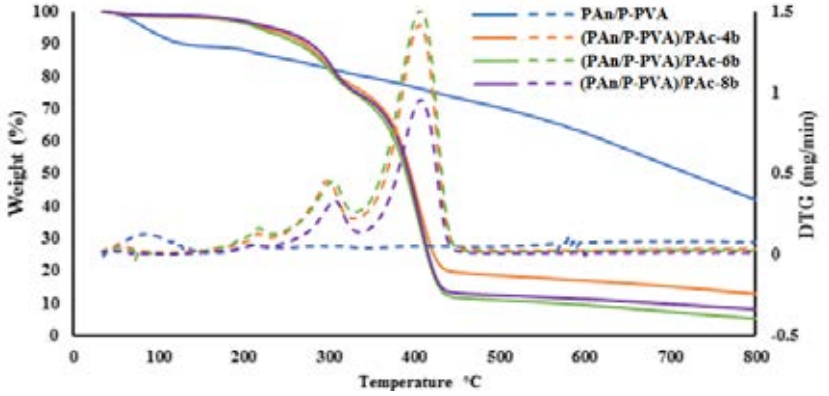

(b) 0.5 g PAn/P-PVA loading

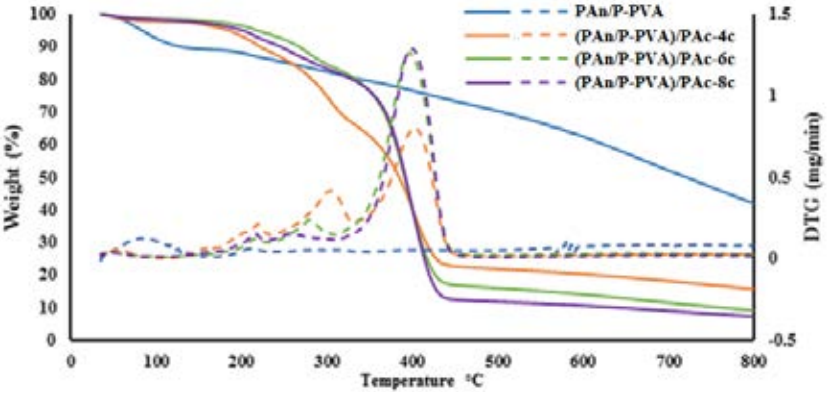

(c) 0.7 g PAn/P-PVA loading

Figure 4.6 TGA (———) and DTA curves (– – –) of (PAn/P-PVA) and (PAn/P-PVA)/PAc nanoparticles: (a) 0.3 g PAn/P-PVA, (b) 0.5 g PAn/P-PVA, (c) 0.7 g PAn/P-PVA loading and 4, 6 and 8 g acrylate amount

4.2.3 XRD Analysis

X-ray diffraction analysis was used to investigate the ordered structure of PAn/P-PVA at 0.3, 0.5 and 0.7 g of PAn/P-PVA loading and 4, 6, 8 g of acrylate amount. The d_{001} values were obtained from XRD patterns as shown in Table 4.4. The alkyl side chains of PAc is reversibly substituted on the PAn/P-PVA backbone through a Coulombic attraction rather than by covalent bond. The non-covalent substitution of a long surfactant alkyl chain tends to enhance the overall anisotropic ordering in PAn/P-PVA. The layered dimensions as observed in the X-ray diffraction patterns of Figure 4.7 indicated that the distance between the main chains is determined by the length of the alkyl chains.

For the PAn/P-PVA, the patterns showed narrow peaks at low angles and broad peak at wide angles. The crystalline peak at $2\theta = 25.35^{o}$ corresponding to layer spacing (*d*-spacing) d_{001} of 0.35 nm was due to the periodicity perpendicular to the polyaniline chain in its emeraldine salt (designated as ES). The results indicated that PAn was partly crystalline [26]. For the (PAn/P-PVA)/PAc, the particles blends with a higher content of the PAc presented strong sharp reflections in the small angle region. The peak at $2\theta = 20^{o}$ was due to the crystallization peaks of PAc overlap with region of a diffused amorphous of the phosphorylate ester side chain of PAn/P-PVA nanoparticles [15]. The positions of the PAn/P-PVA complex peak depended on the PAc concentration, and their intensity decreased with an increasing in PAc concentration. Compared with the PAn/P-PVA, the peaks at $2\theta = 20^{o}$ and 25.3^{o} showed no remarkable change in the XRD pattern of the (PAn/P-PVA)/PAc samples (Figure 4.5), indicating that the crystal structure of the PAn/P-PVA was remained by the encapsulation with the PAc. The driving force for the formation of layered structures is the repulsion between PAn/P-PVA backbone and flexible hydrocarbon side chain. The *d*-spacing corresponding to the first reflection for the different composition of (PAn/P-PVA)/PAc is the interlayer *d*-spacing of the PAn/P-PVA nanoparticles at 0.35 nm. Interestingly, its value increased to 0.4 nm for (PAn/P-PVA)/PAc with addition of PAc. The increase in the interlayer d-spacing of the PAn/P-PVA nanoparticles of small acrylate amount by the expansion of main chains of PAn/P-PVA nanoparticles by introduction of long alkyl chains of PAc. The similar result was earlier reported by Kim M.S.*et al*. [26].

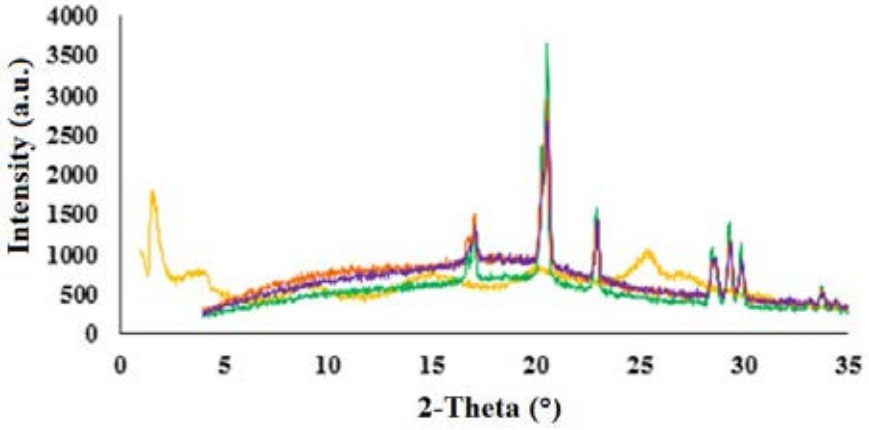

(a) 0.3 g PAn/P-PVA loading

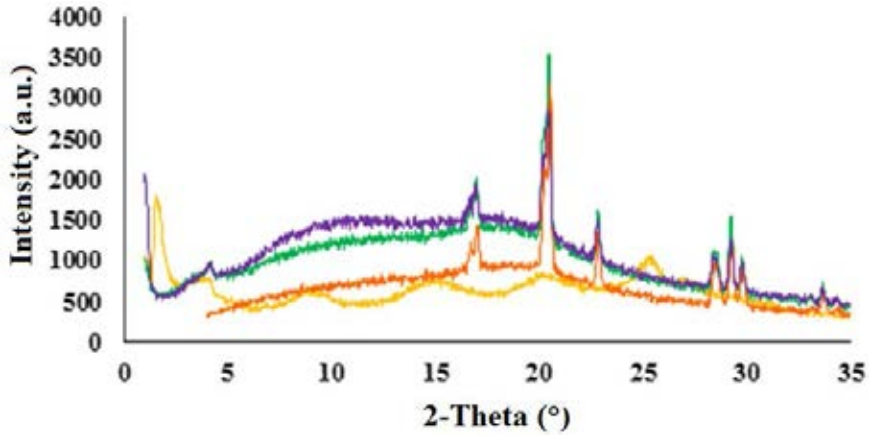

(b) 0.5 g PAn/P-PVA loading

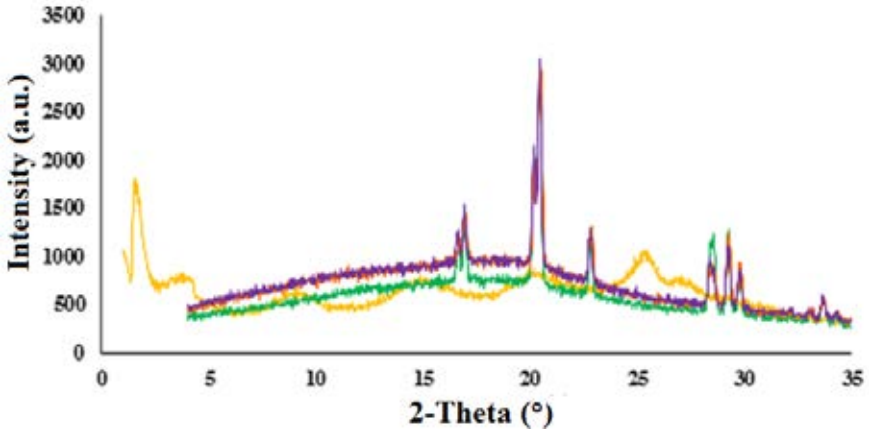

(c) 0.7 g PAn/P-PVA loading

Figure 4.7 XRD patterns of (PAn/P-PVA)/PAc nanoparticles: (a) 0.3 g PAn/P-PVA, (b) 0.5 g PAn/P-PVA, (c) 0.7 g PAn/P-PVA; (——) PAn/P-PVA, (——) (PAn/P-PVA)/PAc-4, (——) (PAn/P-PVA)/PAc-6, (——) (PAn/P-PVA)/PAc-8

Table 4.4 2θ and *d*-spacing of XRD spectra of PAn/P-PVA and (PAn/P-PVA)/PAc nanoparticles

Samples	**2θ (degree)**	**d_{001} (nm)**
PAn/P-PVA	25.35	0.35
0.3 PAn/P-PVA loading		
(PAn/P-PVA)/PAc-4a	20.28	0.437
(PAn/P-PVA)/PAc-6a	20.31	0.437
(PAn/P-PVA)/PAc-8a	20.37	0.436
0.5 PAn/P-PVA loading		
(PAn/P-PVA)/PAc-4b	20.23	0.438
(PAn/P-PVA)/PAc-6b	20.30	0.437
(PAn/P-PVA)/PAc-8b	20.24	0.438
0.7 PAn/P-PVA loading		
(PAn/P-PVA)/PAc-4c	20.46	0.434
(PAn/P-PVA)/PAc-6c	20.49	0.433
(PAn/P-PVA)/PAc-8c	20.44	0.434

4.2.4 Morphology of PAn/P-PVA and (PAn/P-PVA)/PAc Nanoparticles

4.2.4.1 Scanning Electron Microscopy (SEM)

The surface morphologies of PAn/P-PVA and (PAn/P-PVA)/PAc nanoparticles examined by scanning electron microscopy (SEM) are shown in Figures 4.8 and 4.9. The morphology of PAn/P-PVA and (PAn/P-PVA)/PAc nanoparticles prepared by chemical oxidative polymerization and emulsifier-free seeded emulsion polymerization were similar.

From Figure 4.8, SEM image of PAn/P-PVA shows the surface morphology of PAn/P-PVA nanoparticles. It seems to be spherical shape particles with smooth surface. However, some aggregates where most of the particles were bundle of PAn/P-PVA nanoparticles were also formed [15, 33]. The surface morphologies of (PAn/P-PVA)/PAc nanoparticles at various PAn/P-PVA loadings (0.3-0.7 g) and acrylate amounts (4-8 g) were illustrated as shown in Figure 4.9. SEM imaged presented the roughness surface morphologies and aggregation of (PAn/P-PVA)/PAc nanoparticles. At a constant loading of PAn/P-PVA nanoparticles, the roughness of surface morphologies increased with increasing acrylate amount. The larger particle size orientation, indicating that the most of the particles were aggregated with observable bundling. The SEM images also show that the PAn/P-PVA nanoparticles had been encapsulated sufficiently with the large amount of PAc. The appearance of PAn/P-PVA increased with increasing acrylate amount (4-8 g).

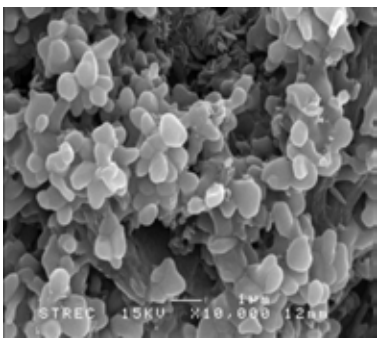

Figure 4.8 Scanning electron micrographs of PAn/P-PVA (10,000x magnification)

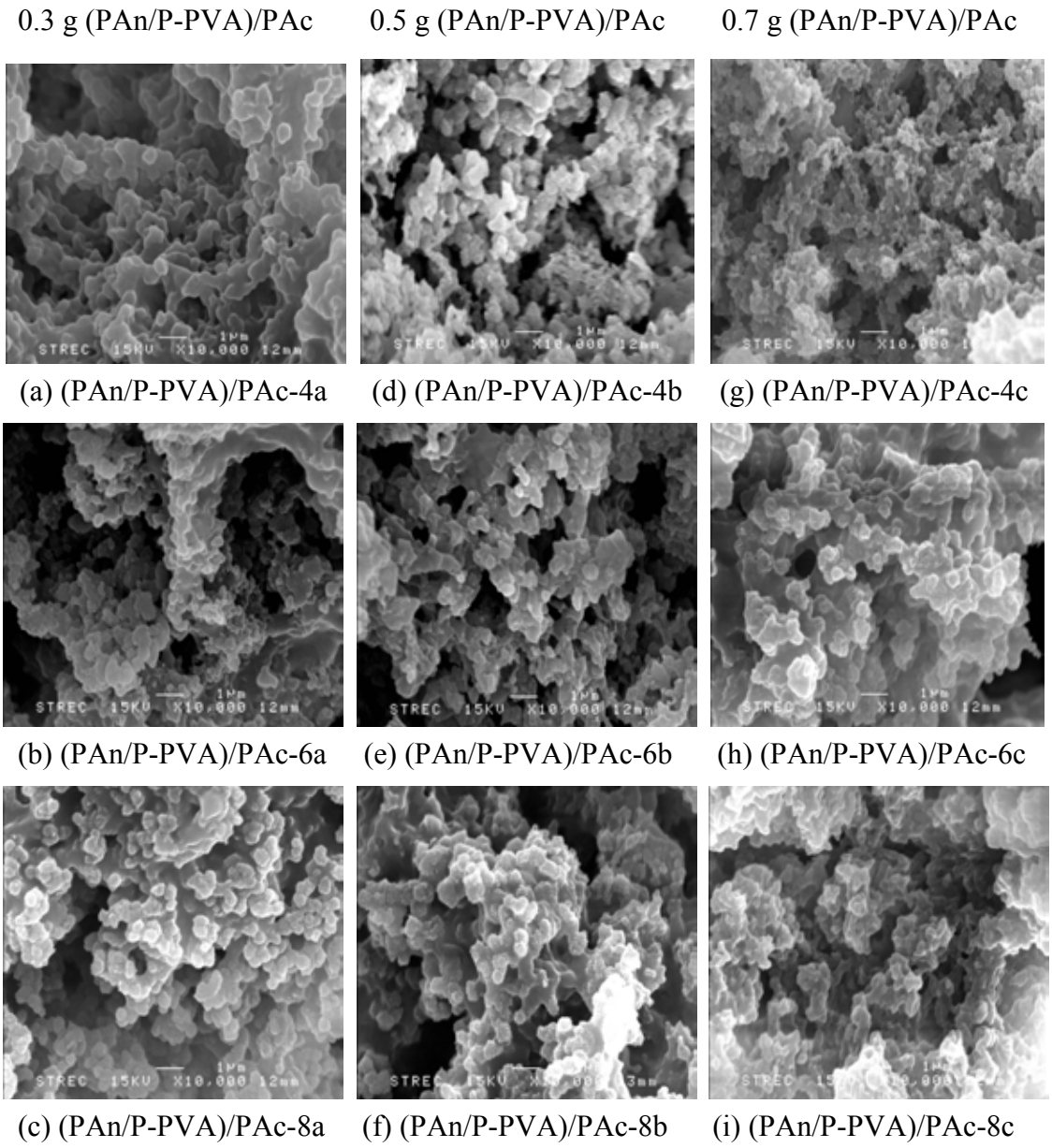

Figure 4.9 SEM of surface morphology of (PAn/P-PVA)/PAc for 0.3, 0.5 and 0.7 PAn/P-PVA loading and 4, 6 and 8 g acrylate amount (10,000x magnification)

4.2.4.2 Transmission Electron Microscopy (TEM)

The morphologies of PAn/P-PVA and (PAn/P-PVA)/PAc nanoparticles examined by TEM micrographs are shown in Figure 4.10 and Figure 4.11 (a-f). OsO_4 can stain only the carbon-carbon double bonds of PAn/P-PVA. This result was similar

to nanosized PAn/P-PVA and (PAn/P-PVA)/PAc prepared via chemical oxidative polymerization and emulsifier-free seeded emulsion polymerization [12, 15].

It was found that the PAn/P-PVA showed a homogenous spherical shape [31] (Figure 4.10) and (PAn/P-PVA)/PAc-4a also showed the similar shape (Figure 4.11a), indicating that there was a small amount acrylate polymerized on the surface of the PAn/P-PVA nanoparticles. The (PAn/P-PVA)/PAc-8a (Figure 4.11d) showed the spherical shape and for the increasing acrylate amount of PAn/P-PVA nanoparticles illustrated rather a strawberry shape [18]. From Figures 4.11a and 4.11d, (PAn/P-PVA)/PAc-4a and (PAn/P-PVA)/PAc-8a showed the same size and strawberry shape of nanoparticles due to PAc formation compared with Figure 4.10. Compared with the PAn/P-PVA, the (PAn/P-PVA)/PAc-b (0.5 g PAn/P-PVA) loading clearly exhibited a strawberry shape with non-smooth surface (Figures 4.11b and 4.11e) due to the PAn/P-PVA encapsulated with PAc. Thus, the shape of nanoparticles changed with increasing acrylate amount.

The dark and light regions on their external corresponded to the PAn/P-PVA and the PAc matrix (latex particles), respectively. TEM images indicated that PAn/P-PVA nanoparticles were partially encapsulated by PAc matrix. Meanwhile, the (PAn/P-PVA)/PAc-4c showed the small particles size and spherical shape and (PAn/P-PVA)/PAc-8c possessed the distinctly larger particles size and irregular shape due to the effective encapsulation of the PAn/P-PVA nanoparticles (Figures 4.11c and 4.11f).

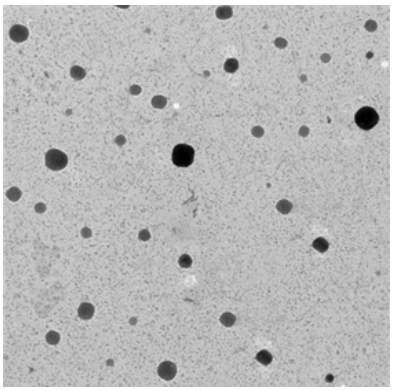

Figure 4.10 Transmission electron micrographs of PAn/P-PVA (x3,000)

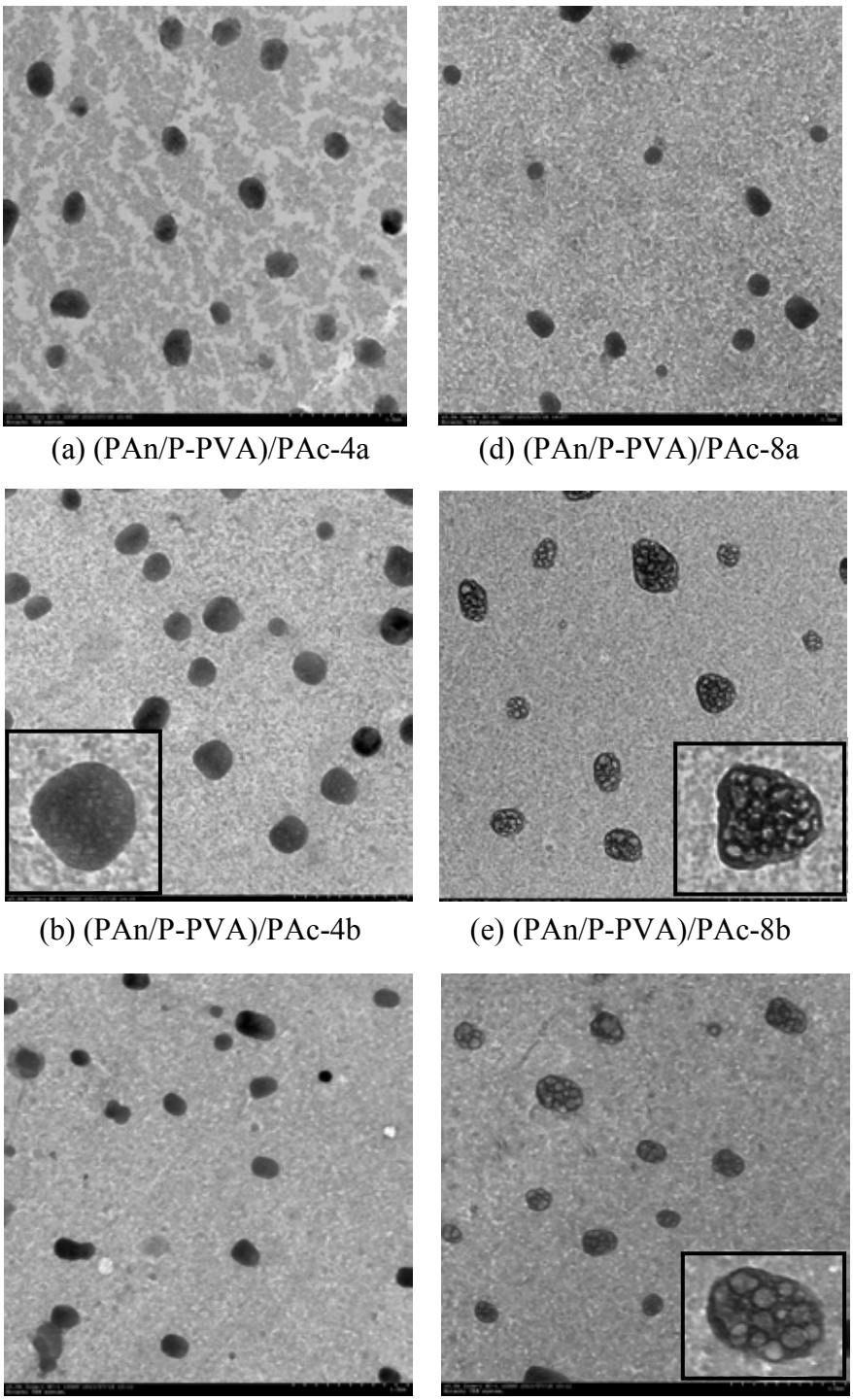

(a) (PAn/P-PVA)/PAc-4a (d) (PAn/P-PVA)/PAc-8a

(b) (PAn/P-PVA)/PAc-4b (e) (PAn/P-PVA)/PAc-8b

(c) (PAn/P-PVA)/PAc-4c (f) (PAn/P-PVA)/PAc-8c

Figure 4.11 Transmission electron micrographs of PAn/P-PVA nanoparticles for 0.3, 0.5 and 0.7 PAn/P-PVA loading and 4 and 8 acrylate amount (x5,000)

4.3 Electroactivity

4.3.1 Cyclic Voltammogram

The PAn/P-PVA and (PAn/P-PVA)/PAc coated on carbon fiber cloth electrodes were subjected to cyclic voltammetry (CV) in the potential range from −1.25 V to +1.25 V at a scan rate of 50 mV/s in the presence of 0.5M HCl aqueous solution, and the results are shown in Figure 4.13.

For the PAn/P-PVA coated on carbon fiber electrode, redox peaks corresponding to the leucoemeraldine form change to protonated emeraldine form and deprotonated emeraldine form change to pernigraniline form could be observed obviously (Figure 4.12) [40]. The sharp redox peaks of PAn/P-PVA occurred faster than that of (PAn/P-PVA)/PAc due to rapid rate of reaction and then oxidation and reduction peak are obvious. As seen in all the voltammograms (Figure 4.13), oxidation peaks were close to each other, this may be due to oxidation reactions of the PAn/P-PVA occurring at close potentials. Also the reduction peaks combined into a single peak because the reaction occurred at similar potentials. Although the reduction peak of PAn/P-PVA were seen together, the reduction peaks of (PAn/P-PVA)/PAc could be seen separately as these materials exhibited less electrical activity compared to PAn/P-PVA. Thus, peaks are shown separately [29]. Finally, it can be noted that the observed differences in the cyclic voltammograms of the (PAn/P-PVA)/PAc and the PAn/P-PVA were an indication of the presence of the acrylic components in the nanocomposites.

Compared with the PAn/P-PVA electrode, there were small differences in the redox peak potentials. For (PAn/P-PVA)/PAc-4a electrode, (Figure 4.13a), the presence of a small amount of PAc had no significant effect on the electrochemical behaviour of the nanocomposites on the electrode. For the (PAn/P-PVA)/PAc-6a electrode, there was an obvious decrease in peak current due to the main surface of the PAn/P-PVA particles coated by the non-conductive PAc. But the separate redox reaction still existed, indicating that the (PAn/P-PVA)/PAc-6a material was electroactive. For the (PAn/P-PVA)/PAc-8a electrode, the peak currents were similar to those of the (PAn/P-PVA)/PAc-6a electrode, suggesting that the (PAn/P-

PVA)/PAc-8a was electroactive due to the fact that the interconnected network between the conducting PAn/P-PVA nanoparticles in (PAn/P-PVA)/PAc-8a was still electroactive. The PAn/P-PVA nanoparticles were encapsulated sufficiently by the non-conductive PAc and the PAc matrix dominantly blocked the electrode surface, which weakened the transfer ability of charges and led to a high resistance of the (PAn/P-PVA)/PAc-8a. It could be concluded that as the loading of acrylate amount increased, the peak current observed during cyclic voltammetry decreased.

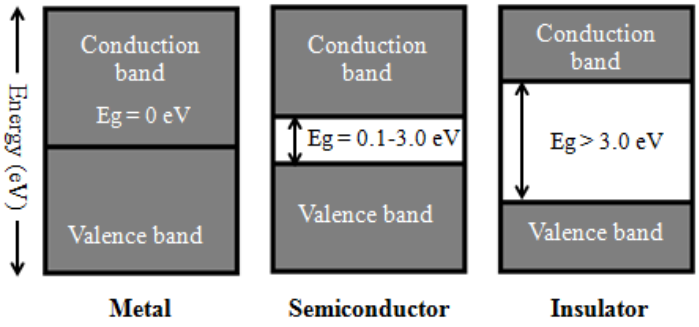

(a)

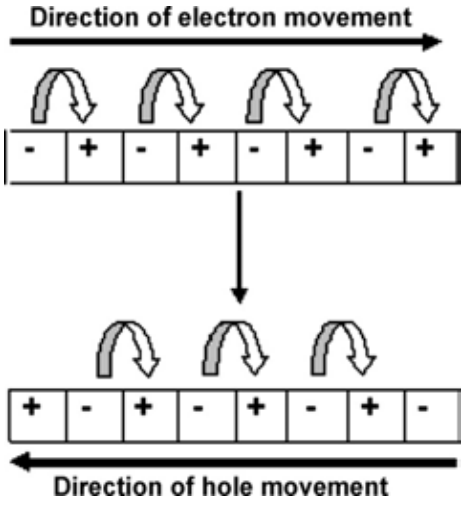

(b)

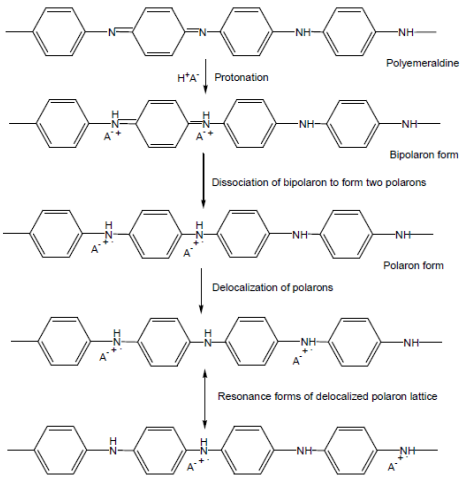

(c)

Figure 4.12 (a) energy band gap diagram [7] (b) conducting parthway of polyaniline [7] and (c) the doping EB with proton to conducting polyaniline form [16]

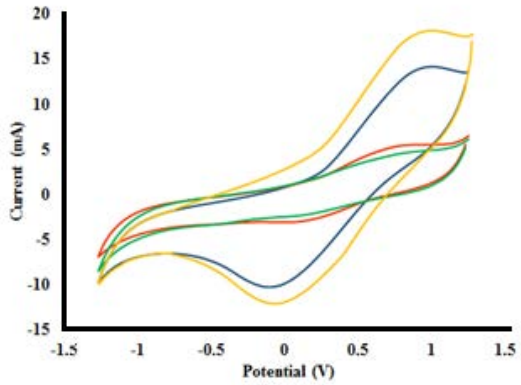

(a) 0.3 g PAn/P-PVA loading

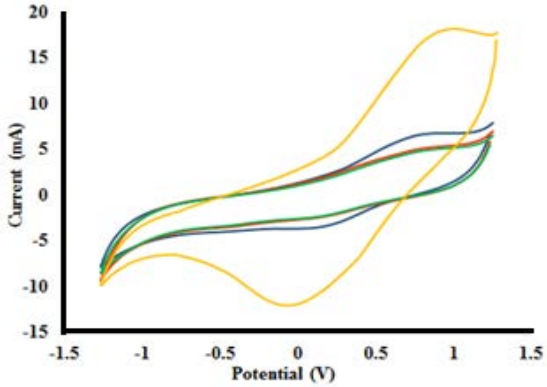

(b) 0.5 g PAn/P-PVA loading

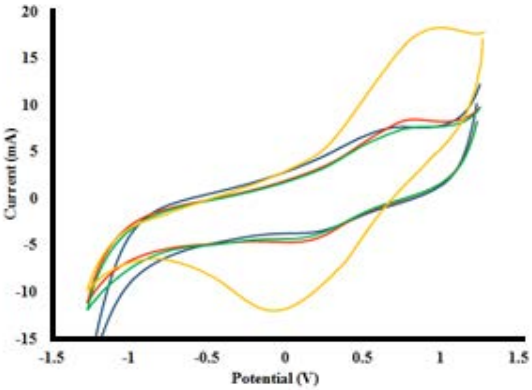

(c) 0.7 g PAn/P-PVA loading

Figure 4.13 Cyclic voltammograms of PAn/P-PVA and (PAn/P-PVA)/PAc nanocomposites coated carbon fiber cloth samples in 0.5M HCl solution; (a) 0.3 g PAn/P-PVA (b) 0.5 g PAn/P-PVA (c) 0.7 g PAn/P-PVA; (———) (PAn/P-PVA), (———) (PAn/P-PVA)/PAc-4, (———) (PAn/P-PVA)/PAc-6, (———) (PAn/P-PVA)/PAc-8

4.4 Corrosion Studies

4.4.1 Tafel Slope Analysis

The electrochemical Tafel slope analysis was used to evaluate the anticorrosive performance of (PAn/P-PVA)/PAc nanocomposites coating on steel samples (Figure 4.14). Tafel plots for (PAn/P-PVA)/PAc nanocomposites coated steel samples were recorded by sweeping the potential from equilibrium potential toward negative and positive potentials against Ag/AgCl reference electrode in 1M H_2SO_4 electrolyte. Figure 4.15 shows Tafel plots for 0.3, 0.5 and 0.7 g loading and 4, 6 and 8 g acrylate amount with 2.25 mm thickness. The steel samples was coated by (PAn/P-PVA)/PAc and soaked in 1M H_2SO_4 solutions [3, 34].

Table 4.5 presents the corrosion potential (E_{corr}), corrosion current (I_{corr}), corrosion rate (CR) and % CR were determined from Tafel plots of coated steel samples in 1M H_2SO_4. For the effect of acrylate amount (4, 6 and 8 g), the current (I_{corr}), corrosion rate and % CR of (PAn/P-PVA)/PAc-8 nanocomposites coated samples were much lower than that of (PAn/P-PVA)/PAc-6 and (PAn/P-PVA)/PAc-4 coated samples at the same of PAn/P-PVA loading. The encapsulated PAc acted as a barrier and non-conductive polymer. Therefore, the incorporation of PAc in PAn/P-PVA matrix promoted the anticorrosive efficiency of coated steel samples. It was also found that the corrosion current (I_{corr}), corrosion rate (CR) and % CR were decreased with an increasing the acrylate amount, as presented in Table 4.5. For the effect of PAn/P-PVA loading (0.3, 0.5 and 0.7 g) at same acrylate amount (0.8 g), the low corrosion current and corrosion rate were observed at high amount of PAn/P-PVA. PAn/P-PVA loading it can be explained that (PAn/P-PVA)/PAc nanocomposites induced the metal oxide formation on steel surface which shifted the corrosion potential of steel to the direction of noble steel and led to a decreasing corrosion current, resulting in the low corrosion current and corrosion rate [29]. The corrosion rate of (PAn/P-PVA)/PAc (0.7 g PAn/P-PVA and 8 g acrylate amount) was similar to the previous work reported by Ali Olad *et al*. [3]

The coating by (PAn/P-PVA)/PAc which PAc acted as a barrier and interface of steel nanocomposites had non-smooth surface, that was tortuosity of diffusion

pathway of corrosion agents such as oxygen gas, hydrogen gas and hydroxide ions. The corrosion rate (CR) of (PAn/P-PVA)/PAc nanocomposites coated on steel samples with various PAn/P-PVA loadings and acrylate amount showed that the best anticorrosive properties of (PAn/P-PVA)/PAc-8c nanocomposites coating was 1.168 mm/year for 0.7 g PAn/P-PVA loading and 8 g acrylate amount. It was lowest corrosion rate over the range of acrylate amount loading (4-8 g) due to the high acrylate amount acted as a barrier property in nanocomposites. For the same amount of acrylate monomer, the corrosion rate decreased with increasing PAn/P-PVA loading. For same PAn/P-PVA loading, the corrosion rate decreased with increasing acrylate amount. Therefore, % CR could be decreased by increasing the amount of both PAn/P-PVA and acrylate amount. For 0.7 g PAn/P-PVA loading with increasing acrylate amount from 4 to 8 g, % CR was decreased from 32.5% to 11.4%. Figure 4.17 also shows that the % corrosion rate decreased with increasing acrylate amount (4, 6 and 8 g) and PAn/P-PVA loading (0.3, 0.5 and 0.7 g). Therefore, the corrosion protection of nanocomposites with 0.7 g with PAn/P-PVA loading nanoparticles encapsulated with 8 g acrylate amount ((PAn/P-PVA)/PAc-8c) showed the best % CR.

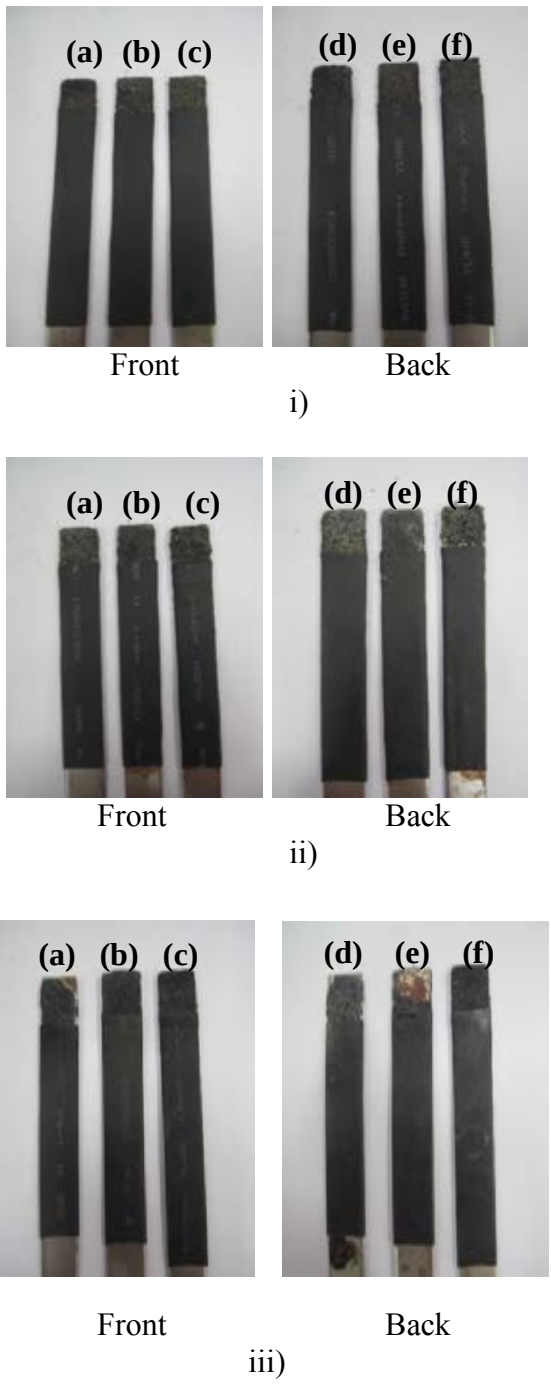

Figure 4.14 Appearance of coated steel coupons of (PAn/P-PVA)/PAc for 0.3, 0.5 and 0.7 g (PAn/P-PVA)/PAc (i-iii) and 4, 6 and 8 g acrylate amount (a, b and c) before and after the electrochemical Tafel slope analysis

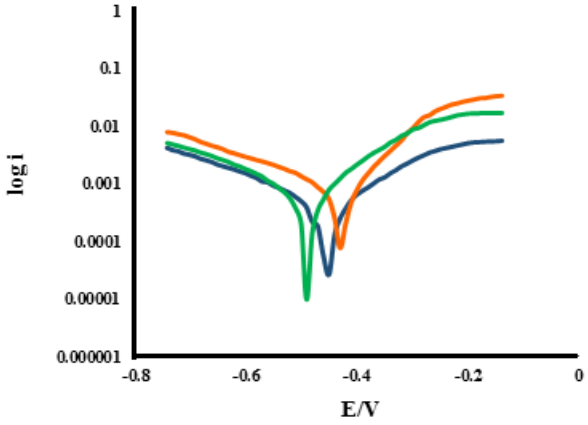

(a) 0.3 g PAn/P-PVA loading

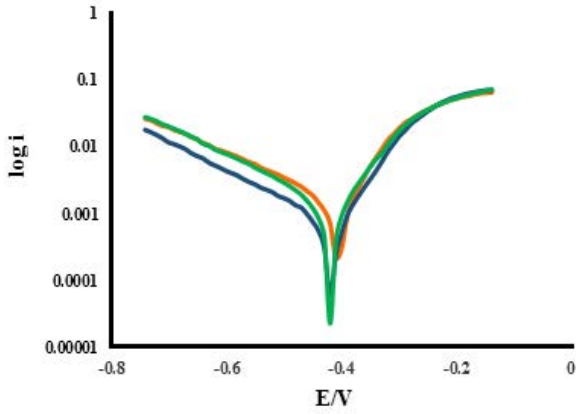

(b) 0.5 g PAn/P-PVA loading

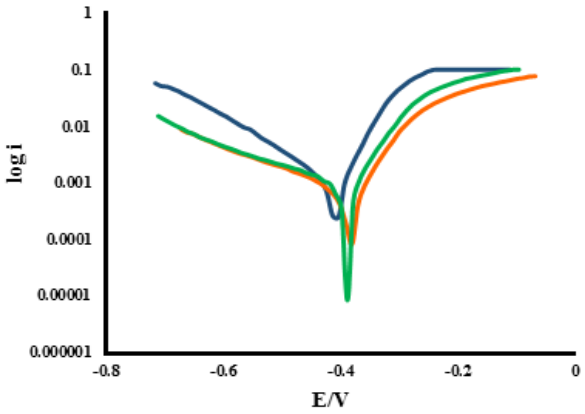

(c) 0.7 g PAn/P-PVA loading

Figure 4.15 Scanning Tafel plots for (PAn/P-PVA)/PAc nanocomposited coated steel sample in 1M H_2SO_4 solution; (a) 0.3 g PAn/P-PVA (b) 0.5 g PAn/P-PVA (c) 0.7 g PAn/P-PVA; (——) (PAn/P-PVA)/PAc-4, (——) (PAn/P-PVA)/PAc-6, (——) (PAn/P-PVA)/PAc-8

Table 4.5 Corrosion potential (E_{corr}), corrosion current (I_{corr}), corrosion rate (CR) and % corrosion rate values calculated from Tafel plots for (PAn/P-PVA)/PAc (0.3, 0.5 and 0.7 g PAn/P-PVA loading and 4, 6 and 8 g acrylate amount) coated steel samples in 1M H_2SO_4 solution.

Sample	**E_{corr} (V)**	**I_{corr} (A/cm^2)**	**CR (mm/year)**	**% CR**
Steel	-0.459	8.769×10^{-4}	10.17	100
0.3 g PAn/P-PVA loading				
(PAn/P-PVA)/PAc-4a	-0.453	2.906×10^{-4}	3.369	33.1
(PAn/P-PVA)/PAc-6a	-0.427	1.789×10^{-4}	2.075	20.4
(PAn/P-PVA)/PAc-8a	-0.487	1.713×10^{-4}	1.986	19.5
0.5 g PAn/P-PVA loading				
(PAn/P-PVA)/PAc-4b	-0.405	2.864×10^{-4}	3.320	32.6
(PAn/P-PVA)/PAc-6b	-0.418	1.582×10^{-4}	1.834	18.0
(PAn/P-PVA)/PAc-8b	-0.417	1.515×10^{-4}	1.757	17.3
0.7 g PAn/P-PVA loading				
(PAn/P-PVA)/PAc-4c	-0.406	2.856×10^{-4}	3.311	32.5
(PAn/P-PVA)/PAc-6c	-0.383	1.461×10^{-4}	1.693	16.6
(PAn/P-PVA)/PAc-8c	-0.388	1.008×10^{-5}	1.168	11.4

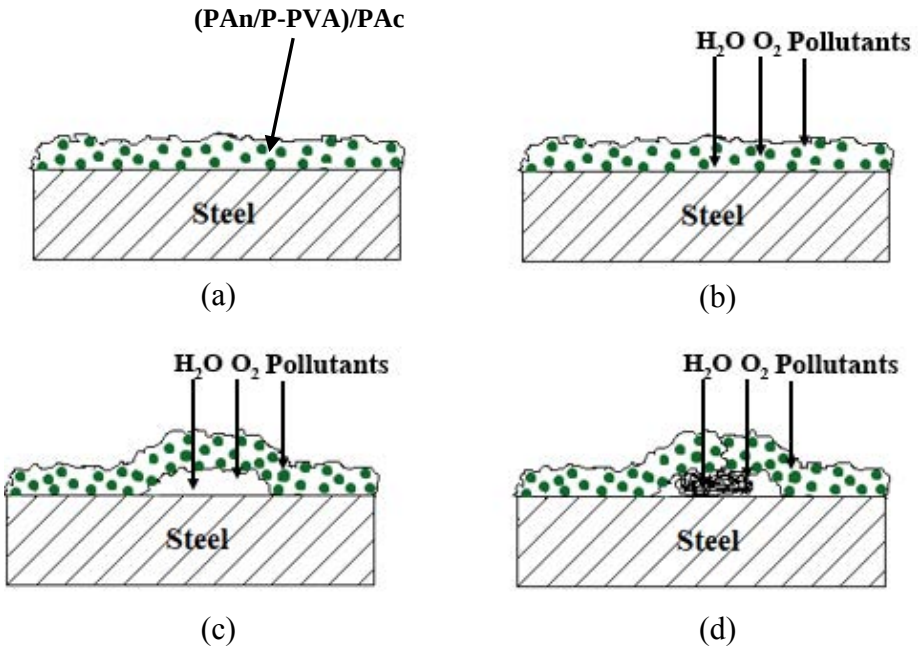

Figure 4.16 Corrosion mechanism of (PAn/P-PVA)/PAc coatings; (a) initial state of the surface, (b) pollutants access, (c) pollutants diffusion and layer swelling and (d) corrosion products obtained under the surface.

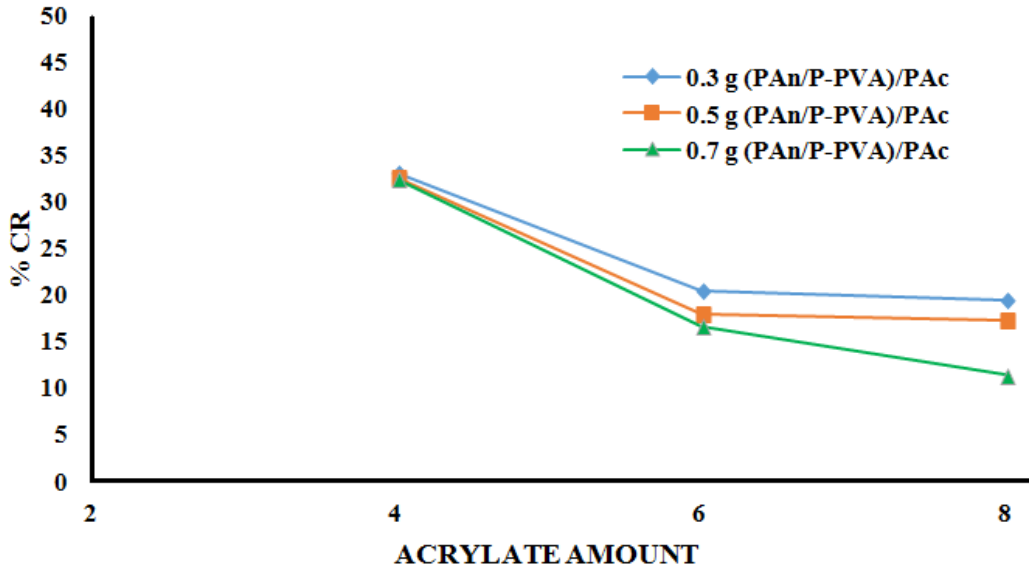

Figure 4.17 Effect of PAn/P-PVA loading and acrylate amount (g) on corrosion rate.

CHAPTER V

CONCLUSIONS AND SUGGESTIONS

5.1 Conclusions

Novel conducting polyaniline nanoparticles encapsulated with polyacrylate were prepared by the emulsifier-free seeded emulsion polymerization. The monomer conversion was decreased, solid content and average particles size were increased with an increasing acrylate amount. The high monomer conversion of 93.9% was achieved at appropriate PAn/P-PVA loading of 0.5 g and 4 g (4.81 %v/v) acrylate monomers. For (PAn/P-PVA)/PAc nanoparticles, at the optimal acrylate amount gave high stability of emulsion with average particle size ($\overline{D}_n$) of 145.7 nm. From thermogravimetric analysis, the thermal stability of the (PAn/P-PVA)/PAc nanoparticles decreased with an increasing acrylate amount, and the maximum degradation temperature of 600°C was achieved resulting in an excellent thermal stability. The increase in PAn/P-PVA interlayer by the addition of small acrylate amount resulted from the expansion of PAn/P-PVA main chain, which was confirmed by X-ray diffraction pattern.

The TEM and SEM micrographs of (PAn/P-PVA)/PAc nanoparticles showed the agglomerated strawberry spheres of PAn/P-PVA with increasing in acrylate amount. From cyclic voltammogram (CV), redox peaks corresponded to the leucoemeraldine/emeraldine form and emeraldine/pernigraniline form. The PAn/P-PVA nanoparticles were encapsulated by the non-conductive PAc and the increase in acrylate amount decreased the redox peak or peak current. From corrosion study in 1.0 M sulfuric acid solution, the results from metal oxide formation on the steel surface induced by coated (PAn/P-PVA)/PAc nanocomposites increased the tortuosity of diffusion pathway of corrosive agents such as oxygen gas, hydrogen gas and hydroxide ions. The (PAn/P-PVA)/PAc-8c nanocomposites showed the best corrosion resistance (CR) of was 11.4%.

5.2 Suggestions of the Future Work

A future investigation of PVA, PAn/P-PVA and (PAn/P-PVA)/PAc nanoparticles should be carried out with the following aspects:

1. Application of colloidal polyaniline dispersion polymerization
   The development of electrical conducting polymeric materials with good flexibility and excellent processability through the improvement of redispersion stability by addition of co-dopant and polymeric stabilizer of polyaniline dispersion polymerization.
2. Ionic conduction in PAn/P-PVA nanoparticles as a polymer electrolytes.
   The preparation of the ionic conducting polymer materials based on PVA and effect of the P-PVA on the ionic conductivity. The carrier mobility and carrier density such as film of P-PVA/poly(ethylene glycol) systems would be further studied.
3. Synthesis of PAn/P-PVA nanoparticles blend with other polymers
   To improve the processability of PAn by blending of PAn composites with easily processable polymers such as poly(butyl methacrylate) (PBMA), poly(styrene-co-styrene sulfonate) (PA/PSS) latex.

REFERENCES

[1] Atta, N.F., Galal, A., and Amin, H.M.A. Synthesis and photoelectrochemical behavior of a hybrid electrode composed of polyaniline encapsulated in highly ordered TiO2 nanotubes array. *Int. J. Electrochem. Sci.* 7 (2012): 3610-3626.

[2] Palaniappan, S., John, A. Polyaniline materials by emulsion polymerization pathway. *Prog. Polym. Sci.* 33 (2008): 732-758.

[3] Olad, A., Naseri, B. Preparation characterization and anticorrosive properties of a novel polyaniline/clinoptilolite nanocomposites *Prog. Org. Coat*. 67 (2010): 233-238.

[4] Wise, D.L., Wnek, G.E., Trantolo, D.J., Cooper, T.M., Gresser, J.D. Electrical and optical polymer systems. New York: Mercel Dekker (1997): 23

[5] "Electrically conductive adhesives." [Online]. Available: http://www.azom.com/article.aspx?ArticleID=6145 [2013, June11]

[6] Aurbach, D. *Industrial Application of Batteries: Characterization of batteries by electrochemical and non-electrochemical techniques.* Netherlands: Elsevier B.V., 2007.

[7] Bhadra, S., Khastgir, D., Singha, N.K., and Lee, J.H. Progress in preparation, processing and applications of polyaniline. *Prog. Polym. Sci.* 34 (2009): 783-810.

[8] Trivedi, D.C. In: Nalwa, H.S., editor. Handbook of organic conductivity molecules and polymers, Wiley; 2 (1997): 592-608, 505-572.

[9] Gospodinova, N., Terlemezyan, L., Conducting polymers prepared by oxidative polymerization: polyaniline. *Prog. Polym. Sci.* 23 (1998): 1443-1484.

[10] An, Y., Koyama, T. Hanabusa K., Shirai, H., Ikeda, J., Yonimo, H., Itoh, T. Preparation and properties of highly phosphorylated poly(vinyl alcohol) hydrogels chemically crosslinked by glutaraldehyde. *Polymer* 36 (1995): 2297-2301.

[11] Takada, N., Koyama, T., Suzuki, M., Kimura, M., Hanabusa, K., Shirai, H., and Miyata, S. Ionic conduction of novel polymer composite films based on partially phosphorylated poly(vinyl alcohol). *Polymer* 43 (2002): 2031-2037.

[12] Chen, F., Liu, P. Preparation of polyaniline/phosphorylated poly(vinyl alcohol) nanoparticles and their aqueous redispersion stability. AIChE J. 57 (2011): 299–605.

[13] Wang, Q., Fu, S., and Yu. T. Emulsion polymerization. *Prog. Polym. Sci. J*. 19 (1994): 703- 753.

[14] Mlynar, M. Chemical binders and auxiliaries. Pennsylvania: Rohm and Haas Company, 2003. (Mimeographed)

[15] Chen, F., Liu, P. Conducting polyaniline nanoparticles encapsulated with polyacrylate via emulsifier-free seeded emulsion polymerization and their electroactive films. *Chem. Eng. J.* 168 (2011): 964-971.

[16] Molapo, M.K., Ndangili, P.M., Ajayi, R.F., Mbambisa, G., Mailu, S.M., Njomo, N., Masikini, M., Baker, P. and Iwuoha, E.I. Electronics of conjugated polymers (I): Polyaniline. *Int. Electrochem. Sci*. *J*. 7 (2012): 11859-11875.

[17] Pernites, R., Ponnapati, R., Felipe, M.J., and A, Rigoberto. Electropolymerization molecularly imprinted polymer (E-MIP) SPR sensing of drug molecules: Pre-polymerization complexed terthiophene and carbazole electroactive monomers. *J. Biosens. Bioelectron.* 26 (2011): 2766-2771.

[18] Zhao, R.J., Jiang, Q., Sun, W., and Jiao. K., Electropolymerization of Methylene Blue on Carbon Ionic Liquid Electrode and Its Electrocatalysis to 3,4-Dihydroxybenzoic Acid. *J. Chinese Chem.* 56 (2009): 158-163.

[19] "Basic overview of the working principle of a potentiostat/galvanostat (PGSTAT) – Electrochemical cell setup." [Online]. Available: http://www.ecochemie.nl/download/Applicationnotes/Autolab Application_Note_EC08.pdf [2011, December 20]

[20] "Chapter II: Theoretical background of electrodeposition, electrochemical supercapacitor and thin film characterization techniques." [Online]. 2012. Available: http://shodhganga.inflibnet.ac.in/bitstream/10603/4057/9/09_chapter%202.pdf

[21] Skotheim, T.A. and Reynolds, J.R. Conjugated Polymers: Processing and Applications. 3rd ed., New York: Taylor & Francis Group, 2007.

[22] Bosich, J.F. Corrosion Prevention for Practicing Engineers. 1970, Barnes & Noble, Inc: New York, US. 1-15.

[23] Chen, F. Liu, P. High electrically conductive polyaniline/partially phosphorylated poly(vinyl alcohol) composite films *via* aqueous dispersions. *Macromol. Res.* 19 (2011): 883-890.

[24] Suzuki, M. Yoshida, T. Koyama, T. Kobayashi, S. Kimura, M. Hanabusa, K. Shirai H. Ionic conduction in partially phosphorylated poly (vinyl alcohol) as polymer electrolytes *Polymer* 41 (2000): 4531-4536.

[25] An, Y. Koyama, T. Hanabusa K. Shirai, H. Ikeda, J. Yoneno, H. Itoh, T. Preparation and properties of highly phosphorylated poly(vinyl alcohol) hydrogels chemically crosslinked by glutaraldehyde. *Polymer* 36 (1995): 2297-2301.

[26] Kim, M.S. Levon, K. Blend of electroactive complexes of polyaniline and surfactant with alkylated polyacrylate. *J. Colloid Interface Sci.*190 (1997): 17-36.

[27] Rout, T.K. Jha, G. Singh, A.K. Bandyopadhyay, N. Mohanty, O.N. Development of conducting polyaniline coating: a novel approach to superior corrosion resistance. *Surf. Coat. Tech.* 167 (2003): 16-24.

[28] Lee, I.S. Cho, M.S. Choi, H.J. Preparation of polyaniline coated poly(methyl methacrylate) microsphere by graft polymerization and its electrorheology. *Polymer*. 46 (2005): 1317-1321.

[29] Coşkun, E. Martìnez-Ramìrez, S.M. Antunez-Flores, W. Hernández-Escobar, C.A. Zaragoza-Contreras, E.A. Improving polyaniline processability by grafting acrylic copolymer. *Synth. Met.* 162 (2012): 344-351.

[30] L.G.B. Bremer, L.G.B. Verbong, M.W.C.G. Webers, M.A.M. van Doorn, M.A.M. Preparation of core-shell dispersions with a low Tg polymer core and a polyaniline shell. *Synth. Met.* 84 (1997): 355-356.

[31] Li, C.Y. Chiu, W.Y. Don, T.M. Polyurethane/polyaniline and polyurethane-poly(methyl methacrylate)/polyaniline conductive core-shell particles: preparation, morphology, and conductivity. *J. Polym. Sci. Part A: Polym. Chem.* 45 (2007): 3902–3911.

[32] Han, M.G. Sperry, J. Gupta, A. Huebner, C.F. Ingram, S.T. Foulger, S.H. Polyaniline coated poly(butyl methacrylate) core–shell particles: roll-to-roll printing of templated electrically conductive structures. *J. Mater. Chem.*17 (2007): 1347-1352.

[33] Lee, I.S., Cho, M.S., and Choi, H.J. Preparation of polyaniline coated poly(methyl methacrylate) microsphere by graft polymerization and its electrorheology. *Polymer* 46 (2005): 1317-1321.

[34] Laco, J.I.I., Villota, F.C., and Mestres, F.L. Corrosion protection of carbon steel with thermoplastic coatings and alkyd resins containing polyaniline as conductive polymer. *Prog. Org. Coat.* 52 (2005): 151-160.

APPENDICES

Appendix A

The Properties of Acrylate monomer and Chemical Composition of the Steel Samples

Table A-1 Properties of Acrylic acid (AA)

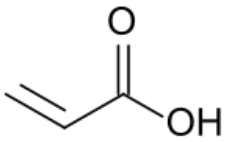

Properties	Acrylic acid
Molecular formula	$C_3H_4O_2$
Molar mass	72.06 g/mol
Density	1.051 g/mL
Melting point	14 °C
Boiling point	141 °C
Appearance	Colorless
Physical form	Clear liquid
Index of refraction, 20 °C	1.4210
Vapor pressure, 25 °C	5.29 hPa

Table A-2 Properties of Ethylene glycol dimethacrylate (EGDMA)

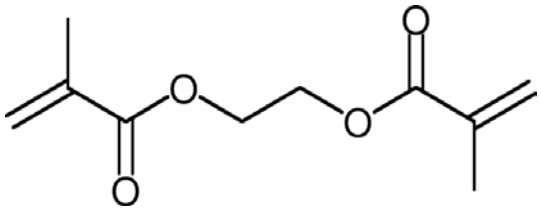

Properties	Ethylene glycol dimethacrylate
Molecular formula	$C_{10}H_{14}O_4$
Molar mass	198.22 g/mol
Density	1.051 g/mL
Boiling point	98-100 °C
Appearance	Colorless
Physical form	Clear liquid
Index of refraction, 20 °C	1.4540
Vapor pressure, 25 °C	1.33 hPa

Table A-3 Properties of Butyl acrylate (BA)

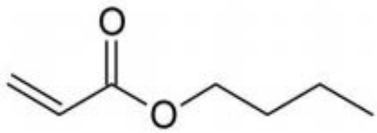

Properties	Butyl acrylate
Molecular formula	$C_7H_{12}O_2$
Molar mass	128.2 g/mol
Density	0.90 g/mL
Melting point	-64 °C
Boiling point	147 °C
Appearance	Colorless
Physical form	Clear liquid
Vapor pressure, 25 °C	7.27 hPa

Table A-4 Properties of Methyl methacrylate (MMA)

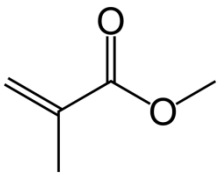

Properties	Methyl methacrylate
Molecular formula	$C_5H_8O_2$
Molar mass	100.12 g/mol
Density	0.94 g/mL
Melting point	-48 °C
Boiling point	101 °C
Appearance	Colorless
Physical form	Clear liquid
Index of refraction, 20 °C	1.414

Table A-5 Chemical composition of the steel spring sheet (SK5)

Element	Percent (w/w, %)
Fe	99.71
Mn	0.25
Cr	0.04

Appendix B

Calculation of Monomer Conversion and Solid Content

$$Monomer\,Conversion(\%) = \frac{M_0 - M_1}{M_2} x100 \quad \text{(B.1)}$$

$$Solid\ content\ (\%) = (M_0 / M_3)\ x\ 100 \quad \text{(B.2)}$$

where; M_0 = Mass of the resulting composite particles (gram)

M_1 = Mass of the charged PAn/P-PVA particles (gram)

M_2 = Mass of the charged acrylate monomer (gram)

$M3$ = Mass of (PAn/P-PVA)/PAc solute (gram)

Table B.1 Monomer conversion calculation and standard deviation

Experiment	PAc loading (g)	M_0 (g)	M_1 (g)	M_2 (g)	% Monomer Conversion
PAn/P-PVA	0	1.9761	0	4	49.40
PAn/P-PVA	0	1.9343	0	4	48.36
PAn/P-PVA	0	1.9863	0	4	49.66
PAn/P-PVA	0	2.0214	0	4	50.54
PAn/P-PVA	0	1.9854	0	4	49.64
PAn/P-PVA	0	1.9240	0	4	48.10
PAn/P-PVA	0	1.9282	0	4	48.21
PAn/P-PVA	0	2.0584	0	4	51.46
PAn/P-PVA	0	2.0401	0	4	51.00
PAn/P-PVA	0	2.0299	0	4	50.75
Mean					49.71
SD					1.21
0.3 g of PAn/P-PVA					
(PAn/P-PVA)/PAc-4a	4	3.3444	0.3	4	76.11
(PAn/P-PVA)/PAc-4a	4	3.0844	0.3	4	74.61
(PAn/P-PVA)/PAc-4a	4	3.3140	0.3	4	75.35
(PAn/P-PVA)/PAc-4a	4	3.5156	0.3	4	80.39
Mean					76.62
SD					2.59
0.3 g of PAn/P-PVA					
(PAn/P-PVA)/PAc-6a	6	4.0174	0.3	6	61.96
(PAn/P-PVA)/PAc-6a	6	4.2357	0.3	6	65.60
(PAn/P-PVA)/PAc-6a	6	3.9547	0.3	6	60.92
(PAn/P-PVA)/PAc-6a	6	4.1326	0.3	6	63.88
Mean					63.09
SD					2.07

Table B.1 Monomer conversion calculation and standard deviation (continued)

Experiment	PAc loading (g)	M_0 (g)	M_1 (g)	M_2 (g)	% Monomer Conversion
0.3 g of PAn/P-PVA					
(PAn/P-PVA)/PAc-8a	8	4.3749	0.3	8	50.94
(PAn/P-PVA)/PAc-8a	8	4.0542	0.3	8	46.93
(PAn/P-PVA)/PAc-8a	8	4.5873	0.3	8	53.60
(PAn/P-PVA)/PAc-8a	8	4.1427	0.3	8	48.04
Mean					49.88
SD					3.00
0.5 g of PAn/P-PVA					
(PAn/P-PVA)/PAc-4b	4	4.3428	0.5	4	96.07
(PAn/P-PVA)/PAc-4b	4	4.2173	0.5	4	92.94
(PAn/P-PVA)/PAc-4b	4	4.3913	0.5	4	97.29
(PAn/P-PVA)/PAc-4b	4	4.0671	0.5	4	89.18
Mean					93.87
SD					3.62
0.5 g of PAn/P-PVA					
(PAn/P-PVA)/PAc-6b	6	5.1350	0.5	6	77.25
(PAn/P-PVA)/PAc-6b	6	4.9230	0.5	6	73.72
(PAn/P-PVA)/PAc-6b	6	5.2836	0.5	6	79.73
(PAn/P-PVA)/PAc-6b	6	5.3020	0.5	6	80.04
Mean					77.68
SD					2.92
0.5 g of PAn/P-PVA					
(PAn/P-PVA)/PAc-8b	8	6.1430	0.5	8	70.54
(PAn/P-PVA)/PAc-8b	8	5.9313	0.5	8	67.90
(PAn/P-PVA)/PAc-8b	8	6.0543	0.5	8	69.43
(PAn/P-PVA)/PAc-8b	8	6.3010	0.5	8	72.52
Mean					70.85
SD					1.94
0.7 g of PAn/P-PVA					
(PAn/P-PVA)/PAc-4c	4	4.1576	0.7	4	86.44
(PAn/P-PVA)/PAc-4c	4	3.9122	0.7	4	80.31
(PAn/P-PVA)/PAc-4c	4	4.2034	0.7	4	87.59
(PAn/P-PVA)/PAc-4c	4	4.2171	0.7	4	87.93
Mean					85.57
SD					3.56
0.7g of PAn/P-PVA					
(PAn/P-PVA)/PAc-6c	6	5.2307	0.7	6	75.52
(PAn/P-PVA)/PAc-6c	6	5.0934	0.7	6	73.23
(PAn/P-PVA)/PAc-6c	6	5.3956	0.7	6	78.26
(PAn/P-PVA)/PAc-6c	6	4.9372	0.7	6	70.62
Mean					74.41
SD					3.26
0.7 g of PAn/P-PVA					
(PAn/P-PVA)/PAc-8c	8	5.9306	0.7	8	65.39
(PAn/P-PVA)/PAc-8c	8	5.8572	0.7	8	64.47
(PAn/P-PVA)/PAc-8c	8	6.2180	0.7	8	68.98
(PAn/P-PVA)/PAc-8c	8	5.7123	0.7	8	62.66
Mean					65.29
SD					2.66

Table B.2 Solid content calculation

Experiment	PAc loading (g)	M_0 (g)	M_3 (g)	% Solid content
PAn/P-PVA	-	1.9761	317	0.6234
PAn/P-PVA	-	1.9343	316	0.6121
PAn/P-PVA	-	1.9863	324	0.6131
PAn/P-PVA	-	2.0214	326	0.6201
PAn/P-PVA	-	1.9854	320	0.6204
PAn/P-PVA	-	1.9240	314	0.6127
PAn/P-PVA	-	1.9282	315	0.6121
PAn/P-PVA	-	2.0584	323	0.6373
PAn/P-PVA	-	2.0401	322	0.6336
PAn/P-PVA		2.0299	319	0.6363
Mean				0.6221
SD				0.01
0.3 g of PAn/P-PVA				
(PAn/P-PVA)/PAc-4a	4	3.3444	86.2178	3.88
(PAn/P-PVA)/PAc-4a	4	3.0844	83.6986	3.69
(PAn/P-PVA)/PAc-4a	4	3.3140	84.2110	3.94
(PAn/P-PVA)/PAc-4a	4	3.5156	83.3547	4.22
Mean				3.93
SD				0.22
0.3 g of PAn/P-PVA				
(PAn/P-PVA)/PAc-6a	6	4.0174	86.4350	4.65
(PAn/P-PVA)/PAc-6a	6	4.1210	87.0521	4.74
(PAn/P-PVA)/PAc-6a	6	3.9547	85.0212	4.66
(PAn/P-PVA)/PAc-6a	6	4.2326	88.5623	4.78
Mean				4.71
SD				0.06
0.3 g of PAn/P-PVA				
(PAn/P-PVA)/PAc-8a	8	4.3749	89.8651	4.87
(PAn/P-PVA)/PAc-8a	8	4.0542	86.7947	4.68
(PAn/P-PVA)/PAc-8a	8	4.5873	92.6240	4.96
(PAn/P-PVA)/PAc-8a	8	4.1427	88.2028	4.70
Mean				4.80
SD				0.14
0.5 g of PAn/P-PVA				
(PAn/P-PVA)/PAc-4b	4	4.3428	88.3614	4.91
(PAn/P-PVA)/PAc-4b	4	4.2173	86.9844	4.85
(PAn/P-PVA)/PAc-4b	4	4.3913	87.0342	5.05
(PAn/P-PVA)/PAc-4b	4	4.0671	86.2341	4.72
Mean				4.88
SD				0.14
0.5 g of PAn/P-PVA				
(PAn/P-PVA)/PAc-6b	6	5.1350	92.0388	5.58
(PAn/P-PVA)/PAc-6b	6	4.9230	89.2631	5.52
(PAn/P-PVA)/PAc-6b	6	5.2836	90.1132	5.87
(PAn/P-PVA)/PAc-6b	6	5.3020	94.2732	5.63
Mean				5.65
SD				0.15

Table B.2 Solid content calculation (continued)

Experiment	PAc loading (g)	M_0 (g)	M_3 (g)	% Solid content
0.5 g of PAn/P-PVA				
(PAn/P-PVA)/PAc-8b	8	6.1430	95.0088	6.46
(PAn/P-PVA)/PAc-8b	8	5.9313	92.1032	6.42
(PAn/P-PVA)/PAc-8b	8	6.0543	91.2319	6.64
(PAn/P-PVA)/PAc-8b	8	6.3010	96.1263	6.56
Mean				6.52
SD				0.10
0.7 g of PAn/P-PVA				
(PAn/P-PVA)/PAc-4c	4	4.1576	86.0300	4.83
(PAn/P-PVA)/PAc-4c	4	3.9122	86.6131	4.52
(PAn/P-PVA)/PAc-4c	4	4.2034	88.1210	4.77
(PAn/P-PVA)/PAc-4c	4	4.2171	87.2645	4.84
Mean				4.74
SD				0.15
0.7 g of PAn/P-PVA				
(PAn/P-PVA)/PAc-6c	6	5.2307	87.0151	6.01
(PAn/P-PVA)/PAc-6c	6	5.0934	85.5193	5.96
(PAn/P-PVA)/PAc-6c	6	5.3956	89.0271	6.06
(PAn/P-PVA)/PAc-6c	6	4.9372	85.0131	5.81
Mean				5.96
SD				0.11
0.7 g of PAn/P-PVA				
(PAn/P-PVA)/PAc-8c	8	5.9306	88.4080	6.71
(PAn/P-PVA)/PAc-8c	8	5.8572	86.2305	6.80
(PAn/P-PVA)/PAc-8c	8	6.2180	90.1394	6.90
(PAn/P-PVA)/PAc-8c	8	5.7123	85.2341	6.79
Mean				6.80
SD				0.08

Appendix C

Appearance of P-PVA, PAn/P-PVA and (PAn/P-PVA)/PAc nanoparticles

(a) (b)

Figure C.1 Appearance of (a) P-PVA (yellow) and (b) P-PVA precipitation in methanol

(a) (b)

Figure C.2 Appearance of (a) colloidal PAn/P-PVA dispersion (b) precipitation of PAn/P-PVA nanoparticles and dry at 40 ^{o}C, 24 h

(a) (b)

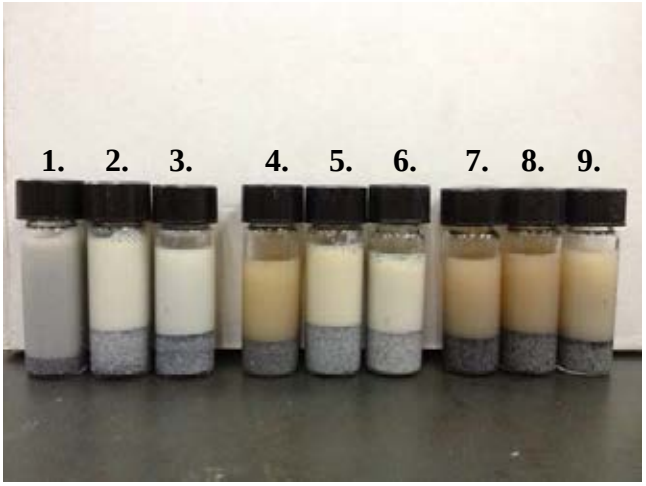

(c)

Figure C.3 Appearance of (a) PAn/P-PVA, (b) PAc and (c) (PAn/P-PVA)/PAc for 0.3 (1-3), 0.5 (4-6) and 0.7 (7-9) (PAn/P-PVA) loading and 4, 6 and 8 g acrylate amount

Appendix D

Working electrode of electrochemical behaviour

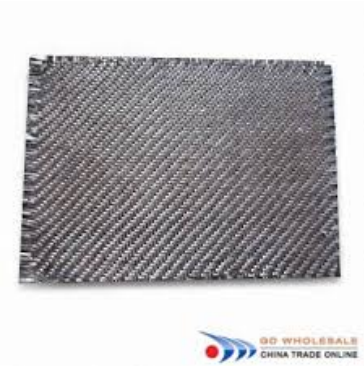

Figure E.1 Carbon fiber cloth

Figure E.2 Nanocomposites coated on carbon fiber

VITA

Miss Phanrapee Varakirkkulchai was born on January 18, 1989 in Bangkok, Thailand. She received her Bachelor's degree of Industrial Chemistry, Kasetsart University. She was admitted to Master Degree in the Program of Petrochemistry and Polymer Science, Chulalongkorn University as student in 2011 and finished her study in 2013.

Presentations at the National Conference

"Conducting Polyaniline Nanoparticles Encapsulated with Polyacrylate via Emulsifier Free Seeded Emulsion Polymerization", October 17-18, 2013. The 3rd Thai Institute of Chemical Engineering and Applied Chemistry International Conference 2013 (The 3rd TIChE 2013), Pullman Khon Kaen Raja Orchid Hotel, Khon Kaen, Thailand